Rate-dependent elastic and elasto-plastic cohesive zone models for dynamic crack propagation

DOI:
10.1016/j.ijsolstr.2016.04.002

Document Version
Accepted author manuscript

Rate-dependent elastic and elasto-plastic cohesive zone models for dynamic crack propagation

S. Salih, K. Davey, Z. Zou

School of Mechanical, Aerospace and Civil Engineering,

The University of Manchester.

Abstract

To overcome deficiencies with existing approaches a new cohesive zone model is introduced and trialled in this paper. The focus is on *rate-dependent* cohesive zone models which have appeared in the recent literature but can be shown to suffer unrealistic behaviour. Different combinations of material response are examined with rate effects appearing either in the bulk material or localised to the cohesive zone or in both. A benefit of using a cohesive-zone approach is the ability to capture plasticity and rate effects locally. Introduced is a categorisation of bulk-material responses and cohesive zone models with particular prominence to the role of rate and plasticity. The shape of the traction separation curve is shown to have an effect and captured in this paper with application of a trapezoidal cohesive zone model. Rate dependency for the cohesive zone model is introduced in terms of a rate-dependent dashpot models applied either in parallel and/or in series. Traditionally, two possible methods are adopted to incorporate rate dependency, which are either via a temporal critical stress or a temporal critical separation. Applied singularly, tests reveal unrealistic crack behaviour at high loading rates. The new rate-dependent cohesive model introduced here couples the temporal responses of critical stress and critical displacement and is shown to provide for a stable realistic solution to dynamic fracture. Dynamic trials are performed on a cracked specimen to demonstrate the capability of the new approach.

Keywords: Cohesive zone model, Traction-separation law, Dynamic loading, Rate dependency

sarmed.salih@postgrad.manchester.ac.uk (S. Salih)

keith.davey@manchester.ac.uk (K. Davey)

zhenmin.zou@manceshter.ac.uk (Z. Zou)

1. Introduction

Monotonic and fatigue crack growth can be modelled by using a method called the Cohesive Zone Model (CZM), which has become the focus of the research in the area of fracture mechanics because of its ability to overcome limitations of other methods founded on linear elastic fracture mechanics (LEFM). The initial concept of the CZM was introduced by Dugdale [1] and Barenblatt [2]. They considered the fracture process zone as a small area ahead of the crack tip, where the normal stress perpendicular to the crack direction of travel is constant and equal to the yield stress according to Dugdale but decreases with deformation and vanishes at separation according to Barenblatt.

The CZM is founded on a traction separation law (TSL) and according to this law, material damage starts when traction reaches a critical value called the critical cohesive stress σ_c. The crack propagates when the displacement jump between the cracked-material surfaces reaches a critical value δ_c at which point the cohesive stress becomes zero and all the cohesive energy Γ_o is dissipated. The CZM gained greater acceptance when Hillerborg et al. [3] analysed numerically, crack-growth in a brittle material using a bilinear cohesive zone model (BCZM) together with the finite element method (FEM). This was followed by Needleman [4], who introduced the polynomial CZM and subsequently, the exponential CZM [5]. Scheider [6] introduced the partly constant CZM, which is similar to Needleman's polynomial model but with a flat region in the middle. The trapezoidal cohesive zone model (TCZM), which is of particular interest in this work, was introduced by Tvergaard & Hutchinson [7]. A bode of contention in the literature is the importance of the shape of the traction separation curve underpinning the cohesive zone approach. Some authors claim that the shape hardly influences fracture simulation results [7–10], whilst other investigations demonstrate that the shape does indeed matter [10–12]. This issue is revisited in this paper by contrasting the trapezoidal cohesive zone model (TCZM) with the bilinear cohesive zone model (BCZM). It is demonstrated that under the constraint of invariant toughness the shape of the traction-separation curve does indeed have an effect.

It is well documented that the CZM in its standard (rate-independent) forms provide an effective approach for the numerical analysis of the failure for a range of materials. This is essentially because of the insensitivity of the crack and certain bulk materials to strain rate and crack velocity. This is not true for all materials however and rate sensitivity can manifest itself in a crack at rate facing greater resistance from the surrounding material along with

other effects such as crack branching. The standard CZM has been found to overestimate crack speeds in the case of dynamic fracture [13]. The predicted crack speed can reach the Rayleigh surface wave speed C_R of the material yet experimentally the maximum crack growth speed is significantly lower than C_R even for very brittle materials [14]. To achieve a better representation of the physics it is necessary to incorporate rate dependency either in the CZM or the bulk material or possibly both. The literature contains examples of research with rate-dependent behaviour in the bulk material combined with a rate-independent traction separation law under monotonically applied loading. Ortiz & Pandolfi [15] for example used this approach and demonstrated good agreement with the experimental data and argued that through this approach the CZM captures the rate dependency of the failure process. Similarly, Song et al. [16] and Zhou et al. [17] successfully applied the approach to asphalt concrete and reinforced aluminium, respectively. Zhou et al. [18] pointed out however that the success of the study of Ortiz & Pandolfi [15] was limited to ductile materials and was successful because of the intrinsic timescale associated with ductility. The approach failed to reproduce existing experimental crack propagation data of pre-strained brittle Polymethyl methacrylate (PMMA). Costanzo & Walton [19] asserted that the rate-independent CZM is unable to represent the experimental results from the literature, regardless of the type of the traction-separation law and the fracture criterion used. A similar conclusion was reached by Langer & Lobkovsky [20] and again Costanzo & Walton [21]. The use of a rate-dependent CZM is therefore recommended [18–21], where the cohesive traction σ is related not just to the crack separation δ, but also to separation rate $\dot{\delta}$, i.e. $\sigma = f(\delta, \dot{\delta})$; a relationship first pioneered by Glennie [22]. Glennie concluded that the reason behind the observed reduction in crack speed with increase in strain rate is an increase in stress levels in the vicinity of the crack tip. Further developments to Glennie's work has been done by Freund et al. [23], Costanzo & Walton [19], [21] and Xu et al. [24]. A negative feature of these approaches however is unrealistically large values for the stress in the cohesive zone and associated crack arrest. A related but alternative approach is adopted by Valoroso et al. [13] and Zhou et al. [18] who employed a CZM with critical traction independent of rate but involving temporal changes in fracture energy along with critical separation. It is demonstrated in this paper however that this approach can lead to unrealistic separation values and crack tearing ahead of the crack tip.

The model proposed in this paper is designed to overcome these identified limitations since it is apparent from the literature that presently no optimum CZM exists that can simulate the

range of crack growth physics met in practice. The CZM used as a vehicle to investigate these issues is introduced in Section 2 and is the trapezoidal model as this is relatively simple and localised plastic behaviour is readily identified. In addition, standard rate-independent CZMs are considered along with different bulk-material models to highlight the limitations of this approach. To achieve a proper understanding of how rate effects can be incorporated into the trapezoidal CZM, relatively benign dashpot models are incorporated into the CZMs in various configurations in Section 3. These models provide a relatively simple vehicle for problem visualisation and assessment of the different types of behaviours. Focus here is on Mode I fracture as this is the most prevalent failure mode in fracture mechanics. An added bonus with dashpot models is that they can facilitate analytical solutions, which can then be explored to great depth. In addition, combinations of bulk material responses with CZMs can readily be assessed. The approach accommodates different localised responses, which is necessary as the behaviour in the cohesive zone can be expected to depart significantly from the original virgin bulk material. Arising out of the analysis in Section 3 is a new rate-dependent model, which is introduced in Section 4. Section 5 focuses on energy transfers invoked by the various dashpot models to provide greater insight into the behaviour of the cohesive zone approach. Discussed in Section 6 is the implementation of the new rate-dependent model arising out of the analysis in previous sections. The new model is incorporated into the commercial software package ABAQUS (via a bespoke UMAT routine) and tested on a cracked specimen subject to different loading rates. The difficulties experienced with existing approaches are shown to be overcome by the new approach.

2. Standard Cohesive Zone models

The cohesive concept is depicted in Figure 1 which depicts a cracked domain and a cohesive zone representing the damage ahead of the crack tip. Also depicted is a tensile element in the cohesive zone whose behaviour is dictated by the trapezoidal traction separation law highlighted in the figure. The trapezoidal cohesive zone model (TCZM) is adopted for this study because it provides reasonable flexibility arising from the extended parameter set $\{\delta_1, \delta_2, \delta_c, \sigma_c\}$. This can be used for example to arrive at the linear cohesive zone model (LCZM) on setting $\delta_1 = \delta_2 = 0$ or the bilinear cohesive zone model (BCZM) with $\delta_1 = \delta_2 \neq 0$ and thus facilitates investigations into the influences of different traction separation curves.

For a pre-defined traction separation law (TSL), two cohesive parameters are usually sufficient to simulate the fracture process. The most frequently used parameters in the

literature are the cohesive-energy or toughness G_c and critical cohesive traction σ_c. The critical separation δ_c can be used in place of G_c but does suffer the disadvantage of not being directly measurable. It is important to appreciate that the cohesive approach is an approach that represents damage as a single-tearing crack, so δ_c is generally not physically observable. The area under the traction separation curve represents the total dissipated energy (per unit area) and typically accounts for energy dissipated due to local plasticity and the energy that is required to form new surface. The ability of the cohesive zone element to represent the local dissipation mechanism of plasticity is a particular advantage of the approach. It provides for example elastic-plastic fracture-mechanics analysis for an elastic-bulk material with the assumption that plasticity is localised at the crack tip. The extent of the plasticity is accounted in the TCZM by the two parameters δ_1 and δ_2. The toughness (fracture energy) G_c is represented by the area under the traction separation curve and is represented mathematically as

$$G_c = \int_0^{\delta_c} \sigma(\delta) d\delta \tag{1}$$

which for the trapezoidal traction-separation law shown in Figure 1 gives

$$G_c = \left(\int_0^{\delta_1} \sigma(\delta) d\delta + \int_{\delta_2}^{\delta_c} \sigma(\delta) d\delta \right) + \int_{\delta_1}^{\delta_2} \sigma(\delta) d\delta = (A_1 + A_3) + A_2 = \Gamma_o + G^{\mathrm{p}} =$$

$$\left(\frac{\sigma_c}{2} \delta_1 + \frac{\sigma_c}{2} (\delta_c - \delta_2) \right) + \sigma_c (\delta_2 - \delta_1) = \frac{\sigma_c}{2} (\delta_2 - \delta_1 + \delta_c) \tag{2}$$

where toughness G_c is the total dissipated energy (i.e. energy dissipated per unit area), G^{p} is the plastic dissipated energy (accounting for local plasticity), Γ_o is the critical cohesive energy (accounting for surface formation), σ is the cohesive traction, σ_c is the critical cohesive traction, δ_1 is the separation at which σ first reaches σ_c, δ_2 is the displacement at which damage is formally assumed to start, and finally δ_c is the critical cohesive separation, at which separation occurs.

The traction separation law depicted in Figure 1 is represented mathematically as

$$\sigma(\delta) = \sigma_c \begin{cases} \frac{\delta}{\delta_1} & if\ 0 < \delta < \delta_1 \\ 1 & if\ \delta_1 \leq \delta \leq \delta_2 \\ \frac{\delta_c - \delta}{\delta_c - \delta_2} & if\ \delta_2 < \delta < \delta_c \end{cases} \tag{3}$$

It is important to appreciate that although this relationship provides the cohesive-energy (per unit area)

$$\Gamma_o = \frac{\sigma_c}{2}(\delta_1 - \delta_2 + \delta_c) \tag{4}$$

and the plastic-energy (per unit area)

$$G^{\mathrm{p}} = \sigma_c(\delta_2 - \delta_1) \tag{5}$$

identified with particular areas under the traction separation curve (see Figure 1), this association is essentially a matter of choice. The association of particular dissipation mechanisms with particular features of the traction separation curve is nothing more than a contrivance. Note also that the region $[0,\ \delta_1]$ is primarily included to avoid an abrupt change in behaviour which can be problematic for some numerical solvers, however, this region is not strictly necessary and does not affect the analysis results. If the model undergoes unloading before reaching the critical stress, then the unloading-path taken is identical to the loading path. Beyond the cohesive critical stress however damage is permanent and consequently the element stiffness decreases. The new stiffness value is $K = \sigma_{max}/\delta_{max}$, where σ_{max} and δ_{max} are the stress and separation at the onset of unloading, respectively. The stress at unloading and reloading is evaluated from $\sigma(\delta) = K\delta$ as depicted in Figure 1.

The theory presented thus far takes no account of time or rate and possible mechanisms for introducing these aspects is discussed in the Section 3 but prior to that it is of interest to examine various bulk-material models incorporating a rate-independent CZM.

2.1 Rate-Independent CZMs

Shown in Figure 1 is a depiction of how the cohesive approach is organised and a particular feature worth highlighting is the material element depicted representing damaged material in the cohesive zone. It is possible to represent the behaviour of this material element by a combination of one-dimensional springs, dashpots, sliders, and cohesive elements. A number of such arrangements of interest in this study are depicted in Figure 2. These can be considered in tandem with 1-D representations of bulk-material responses using similar elements as depicted in Figure 3. Organising material behaviours in this manner provides insight and a certain degree of control and in addition allows for detailed analysis, which can highlight wanted and/or unwanted responses. The cohesive elements depicted in Figure 2 are all derivable from the trapezoidal traction separation law (TSL) on various setting of δ_1

and δ_2. It is of interest to explore and investigate the deficiencies in these simple models to motivate the selection of the final model. In the discussion that follows the bulk-material behaviour is identified by uppercase letters {A, B, C, D} and cohesive models by the lowercase letters {a, b, c, …, p} (see Figure 2 and 3). For example (A-a) refers to a linear material with a linear cohesive element (on setting $\delta_1 = \delta_2 = 0$) and (C-f) means an elastic, rigid-plastic bulk material and a rate-dependent trapezoidal cohesive element. Analysis is restricted to subjecting a prismatic element to displacement δ_o for a range of material models and cohesive element combinations.

Although the main focus in this paper is on the inclusion of rate effects it is insightful also to explore quasi-static loading of rate-independent models to provide a base on which to construct more complex models. The cohesive elements shown in Figure 2 (a, b, c, and d), are rate-independent linear, bilinear, trapezoidal (with $\delta_1 = 0$) and trapezoidal cohesive elements. Recorded in the literature is the successful application of these elements to quasi-static fracture processes for bulk-material Models (A and C) depicted in Figure 3. Limited research [15–17] has been performed on the use of rate-independent cohesive elements with rate-dependent bulk-material models of the type depicted in Figure 3 (B and D). However, this approach has proven insufficient to represent the experimental dynamic crack results (see references [18–21]) and a rate-dependent cohesive model is a possible solution.

2.1.1 Model (A-a)

Combining elements from Figure 3(A) and 2(a) provides the simplest cohesive model consisting of a linear bulk-material and a linear cohesive element. The rate-independent curve in Figure 4(a) shows the stress displacement response. A particular feature of the model is that both the spring and the cohesive part experience the same stress, but strain is additive, i.e. $\sigma_o = \sigma^{\mathrm{e}} = \sigma^{\mathrm{coh}}$ and $\varepsilon_o = \varepsilon^{\mathrm{e}} + \varepsilon^{\mathrm{coh}}$, where ε^{e} is the elastic strain (defined as $\varepsilon^{\mathrm{e}} = \delta^{\mathrm{e}}/l_o$) and $\varepsilon^{\mathrm{coh}}$ is the strain in the cohesive part (defined as $\varepsilon^{\mathrm{coh}} = \delta^{\mathrm{coh}}/l_o$), where l_o is the initial length of a piece of identified material local to and containing an element of the CZ.

Consider an initial displacement δ_o applied to the system and let $\varepsilon_o = \delta_o/l_o$ and $\sigma_o = E\varepsilon_o$, where E is Young's Modulus of the bulk material. If $\sigma_o \leq \sigma_c$, then $\varepsilon_{\mathrm{o}} = \varepsilon^{\mathrm{e}}$, $\sigma = E\varepsilon^{\mathrm{e}}$, $\delta^{\mathrm{e}} = \delta_o = \varepsilon_o l_o$ and the material element behaves like an elastic spring. However, if $\sigma_o > \sigma_c$, then the cohesive element makes a contribution and since the total separation is additive (i.e. $\delta_o = \delta^{\mathrm{e}} + \delta^{\mathrm{coh}}$), the stress can be represented as

$$\sigma^e = \sigma_c \left(1 - \frac{\delta^{coh}}{\delta_c}\right) = E\varepsilon^e = E\frac{\delta^e}{l_o} \tag{6}$$

which can be solved for δ^{e} to give

$$\delta^e = \delta_c \left[\frac{\left(1-\frac{\delta_o}{\delta_c}\right)}{\left(-1+\frac{E\delta_c}{\sigma_c l_o}\right)}\right] \tag{7}$$

which is applicable provided $\delta_o \leq \delta_c$, otherwise the element will fail and the material will separate.

In order to better understand the crack driving force it is insightful to explore energy transfers that take place between the bulk material, cohesive element and the surroundings. In this case $U^e = 0.5\sigma A\delta^{\mathrm{e}}$ and $W^e = U^e/A = 0.5\sigma\delta^{\mathrm{e}}$, where U^e is the elastic strain energy, W^e is the elastic strain energy (per unit area) and δ^{e} is elastic displacement. For $\sigma_o \leq \sigma_c$ the situation is trivial and the total work done by the applied load (per unit area) W^{d} is equal to W^{e}. For $\sigma_o > \sigma_c$ the value of δ^{e} is calculated from Eq. (7) and σ^e from Eq. (6) and the elastic strain energy per unit area is given by $W^e = 0.5\sigma^{\mathrm{e}}\delta^{\mathrm{e}}$ and the energy diverted to material separation is

$$W^\Gamma = \frac{1}{2}(\sigma_c + \sigma^e)\delta^{coh} \tag{8}$$

where W^{Γ} is the cohesive energy per unit area, δ^{coh} is separation at the cohesive element and the total work done (per unit area) is $W^{\mathrm{d}} = W^{\mathrm{e}} + W^{\Gamma}$. Energy dissipation is an important aspect in cohesive models as is apparent in this simple case which features non-recoverable energy W^{Γ}.

2.1.2 Model (B-a)

The addition of a dashpot to the bulk-material model above gives rise to rate-dependent fracture behaviour. In this model stress is identical in the spring, dashpot and cohesive part, but strain is additive and temporal behaviour is a feature, i.e. $\sigma_o = \sigma^{\mathrm{e}} = \sigma^{\mathrm{D}} = \sigma^{\mathrm{coh}}$ and $\varepsilon_o = \varepsilon^e(\mathrm{t}) + \varepsilon^D(\mathrm{t}) + \varepsilon^{\mathrm{coh}}$, where $\varepsilon^e(\mathrm{t})$, $\varepsilon^D(\mathrm{t})$, and $\varepsilon^{\mathrm{coh}}$ are the elastic strain ($\varepsilon^e(\mathrm{t}) = \delta^e(\mathrm{t})/l_o$), the strain in the dashpot at any time ($\varepsilon^D(\mathrm{t}) = \delta^D(\mathrm{t})/l_o$), and the strain in the cohesive element ($\varepsilon^{\mathrm{coh}} = \delta^{\mathrm{coh}}/l_o$) that is irreversible (does not change for fixed δ_o), respectively.

If an initial instantaneous displacement δ_o is applied to this system, then this will result in an initial strain $\varepsilon_o = \delta_o/l_o$ and initial stress $\sigma_o = E\varepsilon_o$. The precise subsequent response of the

system depends on the magnitude of the stress σ_o. If $\sigma_o \leq \sigma_c$, then the cohesive element is not involved and $\dot{\varepsilon}_o = \dot{\varepsilon}^e + \dot{\varepsilon}^D = E^{-1}\dot{\sigma} + \eta^{-1}\sigma$, where η is a material parameter akin to viscosity. With a constant applied displacement $\dot{\varepsilon}_o = 0$ so $E^{-1}\dot{\sigma} + \eta^{-1}\sigma = 0$, which can be solved to provide temporal stress $\sigma(t) = \sigma_o exp(-E\eta^{-1}t)$ and in this case $\sigma(t)$ is always less than σ_c since $\sigma_o \leq \sigma_c$. If on the other hand $\sigma_o > \sigma_c$, then the cohesive element is involved with displacement divided initially between the spring and the cohesive element, i.e. $\delta_o = \delta^e(0) + \delta^{\mathrm{coh}}$, with the dashpot not initially involved. The subsequent response of the model is one of relaxation of stress, since $\sigma^e(t) = \sigma^e(0)exp(-E\eta^{-1}t)$ and the dashpot displacement is obtained from $\dot{\varepsilon}^D(t) = \dot{\delta}^D(t)/l_o = \sigma^e(t)/\eta$, which gives $\delta^D(t) = \delta^e(0)\big(1 - exp(-E\eta^{-1}t)\big)$.

The energy dissipated by the dashpot is evaluated from the rate at which work is done (per unit area) by the stress field, i.e. $\dot{W}_d^D = l_o\sigma^D\dot{\varepsilon}^D$. Substitution of $\sigma^D = \eta\dot{\varepsilon}^D$ and integration gives

$$W^D(t) = \frac{1}{2}\sigma^e(0)\delta^e(0)\left(1 - \left(exp\left(-\frac{E}{\eta}t\right)\right)^2\right) \tag{9}$$

The energy transfers to the system, cohesive element, dashpot and spring are readily determinable with knowledge of the stress and strain rates with total work done (per unit area) satisfying the equation $W^{\mathrm{d}}(t) = W^{\mathrm{e}}(t) + W^{\mathrm{D}}(t) + W^{\Gamma}$. An important aspect of the relaxation process for this model is that δ^{coh} is invariant.

2.1.3 Model (C-a)

Elastic-plastic fracture mechanics is of industrial importance as plasticity provides a mechanism for energy dissipation and consequently increased toughness. One mechanism for incorporating plasticity is to assume an elastic-plastic bulk-material model like that depicted in Figure 3(C). Viscous behaviour is absent in this case and localised softening is achieved with the cohesive element shown in Figure 2(a). The stress-displacement curve for the elastic-plastic material, with a linear cohesive element is shown in Figure 5(a). As with the previous serial models, stress is common to all elements, i.e. $\sigma_o = \sigma^e = \sigma^p = \sigma^{coh}$, and strain is additive, $\varepsilon_o = \varepsilon^{\mathrm{e}} + \varepsilon^p + \varepsilon^{\mathrm{coh}}$. Note also that separation at fracture δ_f has contributions from bulk-material plasticity and the cohesive element, i.e. $\delta_f = \delta^p + \delta_c$. The behaviour of this system depends on the magnitude of the stress σ_o. If $\sigma_o \leq \sigma_Y, \sigma_c$, then elastic behaviour is dominant and the stress will be evaluated from $\sigma_o = \sigma^e$, in this case $\varepsilon^e = \varepsilon_o = \delta_o/l_o$ with

$\delta^e = \delta_o$ and $\mathrm{W^e} = 0.5\sigma_o\,\delta^e$. If however $\sigma_o > \sigma_Y$, with plastic response approximated by the linear expression $\bar{\sigma} = \sigma_Y + E_p\bar{\varepsilon}^{\mathrm{p}}$, where for uniaxial tension effective stress $\bar{\sigma} = \sigma$ and effective plastic strain $\bar{\varepsilon}^{\mathrm{p}} = \varepsilon^p$ (since at this instance it is assumed $\varepsilon^{\mathrm{coh}} = 0$), then the strain $\varepsilon_o = \varepsilon^e + \varepsilon^p$. Consequently, the applied stress to the element can be evaluated as $\delta_o/l_o = \sigma/E + (\sigma - \sigma_y)/E^p$, which is valid when $\sigma \leq \sigma_c$, where E^p is the plastic modulus. Energy is stored elastically but plastic dissipation takes place and is equal to

$$W^p = \frac{1}{2}(\sigma_Y + \sigma)\delta^p \tag{10}$$

where δ^p is the extent of plastic deformation and evaluated from $\delta^p = \delta_o - \delta^e$.

Finally if $\sigma > \sigma_c$, the total strain $\varepsilon_o = \varepsilon^e + \varepsilon^p + \varepsilon^{\mathrm{coh}}$ with $\varepsilon^{\mathrm{coh}} = \delta_c(1 - \sigma^e/\sigma_c)/l_0$, $\varepsilon^p = (\sigma_c - \sigma_y)/E^p$ and $\varepsilon^e = \sigma^e/E$. From this the stress can be evaluated as

$$\frac{\delta_o}{l_o} = \frac{\sigma^e}{E} + \frac{\sigma_c - \sigma_y}{E^p} + \frac{\delta_c\left(1 - \frac{\sigma^e}{\sigma_c}\right)}{l_0} \tag{11}$$

where it is assumed throughout this section that $\sigma_Y < \sigma_c$ because to do otherwise would mean no plastic deformation is possible. Energy is stored elastically but dissipated in terms of plastic dissipation, as it evaluated from Eq. (10) with σ_c replacing σ, and energy dissipated in propagating the crack as it evaluated from Eq. (8). The total work done (per unit area) is $W^{\mathrm{d}} = W^{\mathrm{e}} + W^{\mathrm{p}} + W^{\Gamma}$. The principal feature of this model is the protection offered to the crack through plastic-energy dissipation in the bulk material.

3. Rate-Dependent CZMs

An extraordinarily useful bulk-material model is that of a linear-elastic material depicted in Figure 3(A) and is particularly pertinent if other non-linear behaviours are localised to the crack tip. It is thus of interest to explore the use of a linear-elastic bulk-material model combined with rate-dependent cohesive models suggested in the literature. Combinations involving plastic behaviour in the bulk-material are also of some importance.

3.1 Model (A-i)

Model (A-i) provides rate dependency in the cohesive domain but linear-elastic behaviour in the bulk material. A critical feature of this particular set-up is a critical stress that is a function of the separation rate. An unwelcome aspect is the possible unboundedness of the critical stress. In the parallel part of the model (see Figure 2(i)) the strain is the same and the

stress is additive, but between this portion and the elastic bulk element the stress is identical and the strain is additive. In mathematical terms $\sigma_o = \sigma^e = \sigma^s$, where σ^s is the stress applied to the parallel system and $\sigma^s = \sigma^D + \sigma^{coh}$, $\varepsilon_o = \varepsilon^s(\infty) + \varepsilon^e$ and $\varepsilon^{coh} = \varepsilon^D$, where $\varepsilon^s(\infty) = \lim_{t\to\infty} \varepsilon^s(t)$, is the strain in the parallel system at stationary equilibrium. Observe that for this model the strain ε^{coh} of the cohesive element is now a function of time.

As with previous models if an initial instantaneous displacement δ_o is applied to the system, its response depends on the magnitude of σ_o, where $\varepsilon_o = \delta_o/l_o$ and $\sigma_o = E\varepsilon_o$. If $\sigma_o \le \sigma_c$, then $\delta^e = \delta_o$ and $W^e = 0.5\sigma^e\delta^e$. If on the other hand $\sigma_o > \sigma_c$, then the elastic displacement δ^e is evaluated from Eq. (7) and material separation at stationary equilibrium $\delta(\infty) = \delta_o - \delta^e$ and the stress $\sigma^e = E\delta_e/l_o$. The material separation as a function of time is

$$\delta(t) = \delta(\infty)\left(1 - exp\left(-\frac{E}{\eta}t\right)\right) \tag{12}$$

and the dissipated energy in the dashpot is obtained from

$$W^D(t) = \frac{1}{2}\sigma_o\delta(\infty)\left(1 - \left(exp\left(-\frac{E}{\eta}t\right)\right)^2\right) \tag{13}$$

where the total work done (per unit area) is $W^d(t) = W^e(t) + W^D(t) + W^\Gamma(t)$.

If the rate-dependent fracture energy is defined to be equal to the rate-independent cohesive energy plus the dissipated energy in the dashpot, then the previous equation becomes $W^d(t) = W^e(t) + W^{\Gamma_{rate}}(t)$, where $W^{\Gamma_{rate}}(t)$ is the rate-dependent fracture energy. Furthermore, critical traction can be viewed as a function of separation and separation rate, since $\sigma_c^{rate} = \sigma_c + \sigma^D$. A further common assumption is the linear relationship $\sigma^D = C\sigma_c$, where C is a parameter that is function of separation rate. This returns an expression similar to that has used in reference [25], i.e. the rate-dependent stress relation can then be written as:

$$\sigma_c^{rate}(\dot{\delta}) = \sigma_c(1 + B\dot{\delta}) \tag{14}$$

where *B* is a material parameter reflecting the strength of rate dependency.

By using a similar procedure to the one used in Model (A-a) but with σ_c^{rate} instead of σ_c for the critical cohesive stress the energy transfers in the model can be evaluated.

3.2 Model (A-e)

An alternative possibility for including a dashpot is to use a series combination rather than a parallel one as in the model above. In the case of Model (A-e) a linear rate-independent CE

(i.e. the TCZM with $\delta_1 = \delta_2 = 0$) is selected in series with a dashpot (Figure 2(e)) to form a rate-dependent CE and this element is connected to a linear elastic bulk-material model (Figure 3(A)). The response of the rate-dependent cohesive element can be viewed as a function of the separation speed, since $\delta_{\mathrm{c}}^{\mathrm{rate}} = \delta_{\mathrm{c}} + \delta^D$, where δ_{c} is the rate-independent cohesive separation and δ^D is the dashpot displacement. Setting $\delta^{\mathrm{D}} = C\delta_{\mathrm{c}}$ and on letting $C = B_1\dot{\delta}$ provides

$$\delta_c^{rate}(\dot{\delta}) = \delta_c(1 + B_1\dot{\delta}) \tag{15}$$

which is identical to an expression applied in reference [18] and where B_1 is a material parameter reflecting the strength of rate dependency.

The stress-displacement curve of the rate-independent and the rate-dependent cohesive element is depicted in Figure 4(a). The energy calculation of this model is exactly the same as Model (A-a) apart from using $\delta_{\mathrm{c}}^{\mathrm{rate}}$ instead of δ_{c} to identify the critical separation of the model. An unwelcome feature of the model is the possible unboundedness of $\delta_{\mathrm{c}}^{\mathrm{rate}}$.

3.3 Model (A-g)

Combining the cohesive element shown in Figure 2(g) with the material element shown in Figure 3(A), provides a rate-dependent trapezoidal CE (with $\delta_1 = 0$) in an elastic bulk material. This model is similar to Model (A-e) although an important feature of this model is the incorporation of plastic energy dissipation. In this CE the process zone is separated into a plastic part (represented by the area under the traction separation curve between δ_1 and δ_2) and damage part (represented by the area under the traction separation curve between δ_2 and δ_{c}). For this model the values of δ_1 and δ_2 are selected to be zero and $0.5\delta_{\mathrm{c}}$, respectively. The critical rate-dependent separation $\delta_{\mathrm{c}}^{\mathrm{rate}}$ is assumed to satisfy Eq. (15), which means that when the separation speed increases, the value of the dissipated energy in plastic deformation and in the process of generating new surfaces increases. Figure 4(b) shows the stress-displacement curve of the rate-independent and the rate-dependent cohesive element.

To better understand the behaviour of this model it is prudent to examine what energy transfers take place. Applying displacement δ_o provides $\sigma_o = E\varepsilon_0$ and as with the previous models the system's response depends on the magnitude of this stress. If $\sigma_o < \sigma_c$, then $\delta^e = \delta_o$ and $W^e = 0.5\sigma_0\,\delta^e$. If however $\sigma_{\mathrm{o}} \geq \sigma_{\mathrm{c}}$, then two possibilities arise depending on the magnitude of δ_o. If $\delta_o < \delta_2 + \delta_{max}^{\mathrm{e}}$, with $\delta_{max}^{\mathrm{e}} = \sigma_{\mathrm{c}}/E$, then elastic energy $W^{\mathrm{e}} = \frac{1}{2}\sigma_{\mathrm{c}}\delta_{max}^{\mathrm{e}}$ is constant and the plastic energy dissipated is determined by $W^p = \sigma_c(\delta_o -$

δ^{e}_{max}). Finally, if $\delta_o \geq \delta_2 + \delta^{e}_{max}$, then the crack propagates giving rise to an increase in surface energy and a decrease in the stored elastic energy and no further plastic dissipation.

3.4 Model (C-e)

The model arises from the combination of the cohesive element shown in Figure 2(e) with the material element shown in Figure 3(C) is similar to Model (C-a), but in this model the cohesive element is rate-dependent. In this CE the value of the critical separation δ_c is assumed to be a function of the separation speed, which means that as the separation speed is increased, the value of the dissipated energy in the fracture process increases. Figure 5(a) shows the stress-displacement curve of the rate-independent and the rate-dependent cohesive elements. The energy calculation for this model is similar to Model (C-a) but with δ_c^{rate} from Eq. (15) in place of δ_c.

3.5 Model (C-g)

This model is similar to Model (C-e), but in this model a rate-dependent trapezoidal cohesive element is used as shown in Figure 2(g). In this CE the value of the critical separation δ_c^{rat} is calculated from Eq. (15). As regards the traction separation law, δ_1 is assumed to be zero and δ_2 is set equal to $0.5\delta_c^{rate}$. A feature of this model is that with an increase in separation speed the dissipated energy increases due to plastic deformation and new surfaces formation. Shown in Figure 5(b) is the stress-displacement curve of the rate-independent and the rate-dependent cohesive elements.

4. New Rate-Dependent Cohesive Model

To overcome limitations with existing rate-dependent cohesive model a new model is introduced in this study. A systematic approach has been adopted to better understand the behaviour and limitations of said models and it is expected that any new model should not suffer unrealistic behaviour typically observed with existing approaches. To keep things reasonably simple the bilinear and the trapezoidal cohesive model are incorporated into the new model to simulate the dynamic crack growth processes. A feature of the new model is dashpots in both series and parallel to counter unrealistically high values of δ_c and σ_c observed when dashpots are applied singularly.

4.1 Model (A-m)

The proposed new rate-dependent linear cohesive element is shown in Figure 6(m). The cohesive element consists of two parts one of which is a parallel combination of a rate-independent CE in parallel with a dashpot to provide a rate-dependent critical stress. This part

is active when the rate-dependent cohesive stress is less than the identified stress limit σ_{limit} thus providing a bounded critical stress. The value of σ_{limit} is set so that the area under the traction curve defined by σ_{limit} is equal to an experimentally obtained upper limit on fracture energy. Thus, for $\sigma_c^{rate} < \sigma_{limit}$, Eq. (14) applies and the separation is held constant at the critical separation used for the rate-independent cohesive model. At the point when σ_c^{rate} reaches its limit σ_{limit} this part of the cohesive element becomes inactive and the second part consisting of a series dashpot and rate-independent CE is activated. In this CE the critical stress is equal to σ_{limit} and the critical separation is again equal to that used in the rate-independent model. This part of the cohesive model provides a rate-dependent CE in which the critical stress is constant at σ_{limit} and a critical separation that increases with rate satisfying Eq. (15). The energetic behaviour of this model is similar to Model (A-a) but with using $\sigma_{\mathrm{c}}^{\mathrm{rate}}$ instead of σ_c for $\sigma_o < \sigma_{limit}$ and if $\sigma_o \geq \sigma_{limit}$, then $\delta_{\mathrm{c}}^{\mathrm{rate}}$ is used instead of δ_c. To demonstrate this explicitly consider an initial displacement δ_o applied to this system, and set $\varepsilon_o = \delta_o / l_o$ and $\sigma_o = E\varepsilon_o$. As with previous cases the behaviour of the system depends greatly on the magnitude of σ_o. If $\sigma_o \leq \sigma_{\mathrm{c}}^{\mathrm{rate}}$ (where the inequality $\sigma_{\mathrm{c}}^{\mathrm{rate}} \leq \sigma_{limit}$ is enforced by design), then $\varepsilon_o = \varepsilon^e$, $\sigma = E\,\varepsilon^e$, $\delta^e = \delta_o = \varepsilon_o l_o$ and $W^e = 0.5\,\sigma\,\delta^e$. If on the other hand $\sigma_o > \sigma_{\mathrm{c}}^{\mathrm{rate}}$, then two possibilities arise, i.e. $\sigma_{\mathrm{c}}^{\mathrm{rate}} \leq \sigma_{limit}$ or $\sigma_{\mathrm{c}}^{\mathrm{rate}} > \sigma_{limit}$, where in the latter case critical cohesive stress is set equal to σ_{limit} and $\delta_{\mathrm{c}}^{\mathrm{rate}}$ is used in place of δ_c for energy calculations.

5. Energy Calculations

In this section a numerical description of the energy transfers is presented to support the theoretical descriptions provided in Sections 2 to 4 and to visually highlight the important behaviours found with the different models considered. Moreover, to discover the best formulation for a rate-dependent cohesive zone model a number of dashpot configurations have been considered in combination with a standard rate-independent cohesive element along with the energy transfers involved. The material properties and process parameters selected for the study can be found in Table 1.

Depicted in Figure 7 and 8 is an energy-displacement diagram for a linear rate-independent CE embedded in an elastic bulk material. From Figure 8 it is evident that the crack growth is driven by the stored elastic energy [26]. This is reflected by a decrease in stored elastic energy originating at the point where material separates along with an increase in cohesive energy. The behaviour of this model when a dashpot is added to the bulk material (Model (B-

a)) in order to represent the rate dependency is shown in Figure 9. It is clear from this figure that the response is one of material relaxation rather than a rate-dependent fracture model. This is reflected in the relaxation of stored elastic energy as opposed to driven crack propagation. An alternative is a parallel combination of dashpots to produce a rate-dependent cohesive element as in Model (A-i). In this case however, the dashpot is built into the cohesive element, which implicitly assumes rates local to the crack feature predominantly. The local stress is dependent on the viscosity associated with the dashpot and the rate of separation. This is reflected in the value of the parameter *B* in Eq. (14), which represents the rate dependency of the local damaged material. A particular feature of this model is a critical stress which is not temporally invariant and increases with the separation speed, which could lead to unrealistic crack arrest. The behaviour of this model is shown in Figure 10, where it can be deduced from the rise in energy that the critical stress is increasing with rate. Bearing in mind that critical stress is the damage initiation mechanism in the cohesive model an unrealistically high value can have negative connotations. With this model the critical stress can reach levels significantly higher than the yield stress of the bulk material leading to both crack arrest and unrealistic levels of plastic deformation in any finite element model.

To avoid the possibility of a high critical stress a localised linear dashpot arrangement is an obvious possibility. Model (A-e) is one possibility consisting of a dashpot connected in series with a standard cohesive element, which leads to critical separation being a function to the separation rate of the form of Eq. (15). Although it is claimed in reference [18] that the model can provide more accurate results, it is demonstrated in Section 6 that the model has unrealistic behaviour at high strain rates. Figure 11 shows the energy curves for Model (A-e), where it is apparent that the value of the critical separation is increasing with separation rate leading to high values at very high rates.

It is evident that a new model is necessary to overcome the limitations of both of the previous models. The proposed models considered here for localised rate-sensitive behaviour combines the elastic-bulk material element shown in Figure 3(A) with one of the rate-dependent cohesive elements shown in Figure 6.

A concern however is the effect of plasticity both locally and in the bulk material and therefore it is of interest also to examine models involving the bulk-material model depicted in Figure 3(C). There are numerous approaches for simulating the fracture process in an elastic-plastic material. An example is an elastic-bulk material and plasticity captured locally

in the cohesive element as in Model (A-g) by using the trapezoidal model. This trapezoidal model could be rate-independent or rate-dependent depending on the type of problem. The energy-displacement curve for this model is shown in Figure 12. Alternatively, the problem can be simulated by using the bilinear rate-dependent or rate-independent cohesive model with an elastic-plastic behaviour in the bulk material as in Models (C-a) and (C-e), which provide the results shown in Figure 13 & 14, respectively. Contrasting the results of Model (A-g) (Figure 12) with the result of Model (C-e) (Figure 14) highlights certain distinctive similarities. The advantage of analysis with plasticity captured locally in a CZM is a much reduced analysis cost. However, accuracy is an issue and the benefit of investigating the effect of the TSL and the choice of the TCZM is manifest. In the case of large-plastic deformation taking place in the bulk material, then the advantages of localised plastic analysis are diminished. However, with a view that plastic behaviour in the damaged zone is different from the virgin material then an appropriate cohesive model could be used to improve accuracy. A model of this type is Model (C-g) and the associated energy-displacement curve is depicted in Figure 15.

The energy-displacement plots for the new rate-dependent cohesive element can be found in Figure 16. Contrasting the results in Figure 10, 11 and 16 demonstrates how the new model eliminates the unrealistic behaviour in existing rate-dependent cohesive models. To better demonstrate further the benefits of the new approach the three competing approaches are tested in fracture simulations applied to a CT specimen depicted in Figure 17 in the following section.

6. Monotonic Fracture Simulation in ABAQUS

There are two methods for identifying cohesive behaviour in the commercial finite element solver ABAQUS; the first method is by specifying a cohesive traction between two adjacent surfaces; the main advantage of this method is that ABAQUS will duplicate the nodes at the adjacent surfaces and connect them through cohesive forces. Hence, the thickness of the cohesive zone is approximately zero. The second method is by inserting cohesive elements along the crack path between the bulk material elements, by default the separation width of the cohesive element defaults as unity in ABAQUS making the strain at the cohesive element equal to the separation. The cohesive behaviour in the second type is defined through a cohesive material. This facilitates a user-defined material subroutine, which can be used to specify new non-standard cohesive behaviour of the type considered here.

The types of simulation performed in this study are shown in Table 2. Nine quasi-static simulations are performed on a CT specimen to check the effect of the TSL and the effect of plasticity. Of the nine, two make use of the BCZM and seven utilise the TCZM with associated responses presented in Figure 19 to 20. This is followed by an investigation into the behaviour and the limitations of methods (existing and new) used to capture rate-dependent behaviour. Numerous transient-dynamic simulations have been performed (see Table 2) and details are provided Section 6.2.

6.1 Plasticity Effects

Fracture simulations of a compact tension (CT) specimen which dimensions shown in Figure 17 have been performed in ABAQUS by using the BCZM and repeated using the TCZM; first with an elastic-plastic bulk material and second with an elastic-bulk material. The reason for using these two models is to study the effect of the TSL and to show the benefit of using a CZM to capture plasticity locally. The numerical model consists of 7823 plane-strain elements (type CPE4R) and 100 cohesive elements (type COH2D4) [27]. A mesh sensitivity analysis has been performed which confirms that converged results are attained. Involving a full-integration plane-strain element (CPE4) or increasing the number of elements in the bulk material or the cohesive zone, has little impact on the simulation results presented. The material properties for the bulk material in the numerical simulations are $\{\sigma_y = 280 \text{ MPa}, E = 193 \text{ GPa and } \vartheta = 0.29\}$ with cohesive parameters shown in Table 3.

Shown in Figure 18 & 19 are the plots relating load to load-line displacement (i.e. the reaction force as a function of the applied displacement measured at the loading point represented by the two circular holes shown in Figure 17) for the first two cohesive parameter sets contained in Table 3. It is clear from these plots that the shape of the traction separation curve has a noticeable effect on the load-line curves. This emphasises the importance and influence of the type of TSL and associated cohesive parameters on responses measured remotely from the cohesive zone. The results obtained are for the same specimen using either the BCZM or the TCZM with invariant fracture energy and either critical traction fixed or critical separation fixed. This result is in agreement with the results obtained from many other authors [10]–[12]. Although the results confirm that the TSL can influence fracture behaviour the extent of this influence depends on the geometry and material of the test specimen. If the specimen has high stiffness, then greater sensitivity to the shape of the TSL can be anticipated [10]. This point is made explicit in Figure 20, where load-line displacement curves can be found for fracture simulations by using the cohesive parameter set

number 3 and 4 (see Table 3.) contrasting TSLs in an elastic-plastic bulk material against a purely elastic bulk material. From these curves, it is clear that the TCZM displays a clear elastic-plastic response making it more appropriate than the BCZM for simulating fracture for an elastic-plastic bulk material yet adopting only an elastic material for the analysis. It is clear from Figure 20 that the TCZM gives a wide range of responses depending on the cohesive parameters used.

6.2 Strain Rate Effect

In this section the rate-dependent CZM is used to simulate the fracture behaviour of a CT specimen subjected to different applied loading speeds. For each loading speed a number of simulations are performed which are: (i) rate-independent BCZM and TCZM; (ii) stress rate-dependent BCZM and TCZM (i.e. critical stress is function of separation rate), (iii) separation rate-dependent BCZM (i.e. critical separation is function of separation rate) and finally; (iv) the new rate-dependent BCZM and TCZM (i.e. the new approach proposed in this study). To enable crack length to be defined, the crack tip is identified at a position where separation equals the critical cohesive separation. Shown in Figure 21 to 24 are plots revealing the temporal response of crack length for the existing rate-dependent approaches with the BCZM at four loading speeds i.e. 0.1, 1.0, 10 and 100 m/s, respectively. At the lowest rate it is apparent on examination of Figure 21 that there is little difference between the rate-independent and rate-dependent models. Increasing the loading rate however reveals a decreasing rate of crack growth (see Figure 22 to 24). Examination of Figure 23 and 24 at respective loading speeds of 10 m/s and 100 m/s reveals unexpected and somewhat unrealistic behaviour with crack initiating not at the crack tip but at a point inside the specimen and subsequently propagating in two directions (see Figure 25 & 26). This behaviour is as a consequence of the strain rate at elements in the location of the crack tip being much higher than elsewhere and consequently giving rise to a very high critical separation. A feature of the highest loading rate of 100 m/s, for the separation rate-dependent CZM is a delay in the initiation of the crack subsequently followed by rapid growth (see Figure 24). This behaviour can be observed in brittle materials such as Polymethyl methacrylate; see reference [18] for example. However both existing rate models lead to unrealistic crack arrest at high loading rates and the separation rate-dependent model suffers greatest in this regard.

A feature of the new rate model described in Section 5 is a bounded critical stress which if correctly set should prevent unrealistic crack arrest (in this study this value was set to 4 times the yield stress). Moreover, following the reaching of this upper bound any further increase

in fracture energy is as a consequence of increases in critical separation. The behaviour of the new rate model is outlined schematically in Figure 27. Although there is insufficient experimental data in the literature to allow a direct comparison there is however evidence for an increase in the fracture energy with rate; see for example the experimentally-obtained curve for G_{ic} from reference [28] and reproduced in Figure 28. It is evident that fracture energy does not increase without bound which is an unrealistic feature of existing models. The upper limit for fracture energy can be determined experimentally but in the absence of this data a limit of 2.5 times the rate-independent fracture energy is applied. The results obtained from the simulation of the fracture process for the CT specimen depicted in Figure 17 with the new model in comparison with existing models are shown in Figure 29 and 30. It is evident from these figures that the new model provides results close to the results obtained with the stress rate-dependent model but without a high critical-stress value. The critical stress at the first element in the stress rate-dependent model reaches 2600 MPa at a 10 m/s loading speed as shown in Figure 31 and 3000 MPa at 100 m/s as shown in Figure 32, These values are incredibly high and provides unrealistic responses. This unrealistic behaviour is eliminated by the new model as shown in Figure 33. The result of the simulation using the TCZM is different from the BCZM and provides further evidence that the type of TSL has an effect (see Figure 29 & 30). Note that the same fracture energy and critical stress were used in the simulation.

For all the rate-dependent models the rate dependency is a function of the rate of separation and a constant parameter (B) (and the parameter B_1 for the new model only) and affects the strength of rate dependency in the material. In practice, these two parameters would be determined by curve fitting experimentally-obtained results. Figure 34 shows the effect of the parameter B on the crack growth speed for the stress rate-dependent and the new rate-dependent model for both BCZM and TCZM, since with increasing its value the crack growth speed is decreasing. The value of the parameter B_1 is observed to have a minor effect on the crack growth speed for reasonable values of σ_{limit}. Investigations for B_1 equated to any one of the values {0.126, 0.166, 0.206, 0.246} reveals little effect at loading speeds of 10 m/s and 100 m/s. This is not too unexpected since increasing the value of σ_{limit} for an invariant fracture energy has the effect of diminishing the influence of δ_c^{rate}. A parametric study has been carried out to check the sensitivity of the model to small changes in material properties, σ_{limit} and the upper bound on fracture energy, i.e. $W_{limit}^{\Gamma\,\text{rate}}$. A range of values between 190 to 200GPa for elastic modulus and 0.29 to 0.33 for the Poisson's ratio has negligible impact on

the simulation results. Although a value for $W_{limit}^{\Gamma\,\mathrm{rate}}$ can be obtained experimentally and used to set σ_{limit}, it is of interest to explore the decoupling of this relationship. The response obtained for the situation where σ_{limit} is relatively high compared to the value obtained from $W_{limit}^{\Gamma\,\mathrm{rate}}$ is shown in Figure 35. In this case the model reduces to the behaviour observed in a rate-independent cohesive model with σ_c set by $W_{limit}^{\Gamma\,\mathrm{rate}}$ and rate-independent δ_c applied to all the cohesive elements. Shown in Figure 36 however is the behaviour, where σ_{limit} is much less than the value obtained from $W_{limit}^{\Gamma\,\mathrm{rate}}$, which is similar to that observed with the displacement rate-dependent cohesive model. It is evident that coupling σ_{limit} to $W_{limit}^{\Gamma\,\mathrm{rate}}$ provides for a stable cohesive zone model.

7. Conclusion

- The type of TSL can have a measurable effect on the results of any fracture simulation.
- The TCZM is able to capture the effects of plasticity local to the CZ and can be used with an elastic or elastic-plastic bulk material.
- Existing methods employed to account for rate-sensitivity in fracture processes have been shown to suffer from certain deficiencies including unrepresentative values of critical stress and separation.
- To overcome these limitations a new rate-dependent CZM has been trialled, which connects the rate-dependent fracture energy to critical stress and separation in a manner that ensures critical cohesive stress remains bounded and critical separation attains lower values than with competing methods.
- The new rate-dependent CZM model has been shown to provide acceptable results and provides for enhanced stability when contrasted against competing methodologies.
- The rate-dependent behaviour of the new model is dependent on two parameters {B, B_1}. It was found that an increase in B decreases crack-growth speed with B_1 having only a minor influence on crack growth behaviour for typical values of bounds on critical cohesive stress.

Acknowledgements

The authors would like to acknowledge the Higher Committee for Education Development in Iraq and the College of Engineering at Babylon University for providing support for Sarmed Salih to facilitate his doctoral research at the University of Manchester.

Reference

[1] D. Dugdale, “Yielding of steel sheets containing slits,” *J. Mech. Phys. Solids*, vol. 8, no. 2, pp. 100–104, 1960.

[2] G. I. Barenblatt, “The mathematical theory of equilibrium cracks in brittle fracture,” *Adv. Appl. Mech.*, vol. 7, no. 1, pp. 55–129, 1962.

[3] A. Hillerborg, M. Modéer, and P. Petersson, “Analysis of crack formation and crack growth in concrete by means of fracture mechanics and finite elements,” *Cem. Concr. Res.*, vol. 6, pp. 773–782, 1976.

[4] A. Needleman, “A continuum model for void nucleation by inclusion debonding,” *J. Appl. Mech.*, vol. 54, no. September, pp. 525–531, 1987.

[5] A. Needleman, “An analysis of tensile decohesion along an interface,” *J. Mech. Phys. Solids*, vol. 38, no. 3, pp. 289–324, Jan. 1990.

[6] I. Scheider, “Cohesive model for crack propagation analyses of structures with elastic–plastic material behavior Foundations and implementation,” *GKSS Res. Cent. Geesthacht, Dept. WMS*, 2001.

[7] V. Tvergaard and J. W. Hutchinson, “The relation between crack growth resistance and fracture process parameters in elastic-plastic solids,” *J. Mech. Phys. Solids*, vol. 40, no. 6, pp. 1377–1397, Aug. 1992.

[8] A. Needleman, “An analysis of decohesion along an imperfect interface,” *Int. J. Fract.*, vol. 42, no. 1, pp. 21–40, 1990.

[9] T. Siegmund and A. Needleman, “A numerical study of dynamic crack growth in elastic-viscoplastic solids,” *Int. J. Solids Struct.*, vol. 34, no. 7, pp. 769–787, Mar. 1997.

[10] G. Alfano, S. De Barros, L. Champaney, and N. Valoroso, “Comparison Between Two Cohesive-Zone Models for the Analysis of Interface Debonding,” *Eur. Congr. Comput.*

Methods Appl. Sci. Eng., pp. 1–18, 2004.

[11] M. L. Falk, A. Needleman, and J. R. Rice, “A critical evaluation of dynamic fracture simulations using cohesive surfaces,” p. 8, 2001.

[12] X. Zhang, Y.-W. Mai, and R. G. Jeffrey, “A cohesive plastic and damage zone model for dynamic crack growth in rate-dependent materials,” *Int. J. Solids Struct.*, vol. 40, no. 21, pp. 5819–5837, Oct. 2003.

[13] N. Valoroso, G. Debruyne, and J. Laverne, “A cohesive zone model with rate-sensitivity for fast crack propagation,” *Mech. Res. Commun.*, pp. 8–13, Jan. 2014.

[14] K. Ravi-Chandar, “Dynamic fracture of nominally brittle materials,” *Int. J. Fract.*, vol. 90, no. 1901, pp. 83–102, 1998.

[15] M. Ortiz and A. Pandolfi, “Finite-deformation irreversible cohesive elements for three-dimensional crack-propagation analysis,” *Int. J. Numer. Methods Eng.*, vol. 44, pp. 1267–1282, 1999.

[16] S. H. Song, G. H. Paulino, and W. G. Buttlar, “A bilinear cohesive zone model tailored for fracture of asphalt concrete considering viscoelastic bulk material,” *Eng. Fract. Mech.*, vol. 73, no. 18, pp. 2829–2848, Dec. 2006.

[17] F. Zhou, J.-F. Molinari, and Y. Li, “Three-dimensional numerical simulations of dynamic fracture in silicon carbide reinforced aluminum,” *Eng. Fract. Mech.*, vol. 71, no. 9–10, pp. 1357–1378, Jun. 2004.

[18] F. Zhou, J.-F. Molinari, and T. Shioya, “A rate-dependent cohesive model for simulating dynamic crack propagation in brittle materials,” *Eng. Fract. Mech.*, vol. 72, no. 9, pp. 1383–1410, Jun. 2005.

[19] F. Costanzo and J. Walton, “Numerical simulations of a dynamically propagating crack with a nonlinear cohesive zone,” *Int. J. Fract.*, vol. 91, no. 4, pp. 373–389, 1998.

[20] J. S. Langer and A. E. Lobkovsky, “Critical examination of cohesive-zone models in the theory of dynamic fracture,” *J. Mech. Phys. Solids*, vol. 46, no. 9, pp. 1521–1556, Sep. 1998.

[21] F. Costanzo and J. R. Walton, “A study of dynamic crack growth in elastic materials using a cohesive zone model,” *Int. J. Eng. Sci.*, vol. 35, no. 12–13, pp. 1085–1114, Sep. 1997.

[22] E. Glennie, “A strain-rate dependent crack model,” *J. Mech. Phys. Solids*, vol. 19, no. 5, pp. 255–272, 1971.

[23] L. B. Freund and Y. J. Lee, “Observations on high strain rate crack growth based on a strip yield model,” *Int. J. Fract.*, vol. 42, no. 3, pp. 261–276, Mar. 1990.

[24] D. B. Xu, C. Y. Hui, E. J. Kramer, and C. Creton, “A micromechanical model of crack growth along polymer interfaces,” *Mech. Mater.*, vol. 11, no. 3, pp. 257–268, May 1991.

[25] D. Kubair, P. Geubelle, and Y. Huang, “Analysis of a rate-dependent cohesive model for dynamic crack propagation,” *Eng. Fract. Mech.*, vol. 70, no. 5, pp. 685–704, 2002.

[26] H. Dahlan, “A Fast-Track Method for Fatigue Crack Growth Prediction with a Cohesive Zone Model,” University of Manchester, 2013.

[27] *ABAQUS 6.13 User Guide*. USA: Dassault Systèmes Simulia Corp, 2013.

[28] S. Marzi, O. Hesebeck, M. Brede, and F. Kleiner, “A Rate-Dependent Cohesive Zone Model for Adhesively Bonded Joints Loaded in Mode I,” *J. Adhes. Sci. Technol.*, vol. 23, no. 6, pp. 881–898, Jan. 2009.

Appendix 1: Energy Transfers in Model (B-a)

This section focuses on a particular 1-D model to provide an illustration of how energy flows can be determined analytically under the assumption of small deformation theory. Consider then Model (B-a) being subjected to an instantaneous strain $\varepsilon_o = \delta_o/l_o$ to give $\sigma_o = \sigma_e = \sigma_D = \sigma_{coh}$ and $\varepsilon_o = \varepsilon^e_{(t)} + \varepsilon^D_{(t)} + \varepsilon_{coh}$, with δ_o independent of time and $\sigma_o = E\varepsilon_o$. The strains $\varepsilon^e_{(t)}$, $\varepsilon^D_{(t)}$, and ε_{coh} are the elastic strain at any time ($\varepsilon^e_{(t)} = \delta^e_{(t)}/l_o$), the strain in the dashpot at any time ($\varepsilon^D_{(t)} = \delta^D_{(t)}/l_o$), and the strain in the cohesive zone ($\varepsilon_{coh} = \delta/l_o$), which is irreversible (does not change for fixed δ_o). The behaviour of this system depends on the relative magnitudes of σ_o and σ_c.

If $\sigma_o \leq \sigma_c$, then $\delta^e_{(t)} = \delta_0 - \delta^D_{(t)}$ and $\dot{\varepsilon}_o = \dot{\varepsilon}^e + \dot{\varepsilon}^D = E^{-1}\dot{\sigma} + \eta^{-1}\sigma$ with $\dot{\varepsilon}^e = \dot{\delta}^e/l_o$ and $\dot{\varepsilon}^D = \dot{\delta}^D/l_o$. With $\dot{\varepsilon}_o = 0$, stress is obtained on integration of $\dot{\varepsilon}_o = E^{-1}\dot{\sigma} + \eta^{-1}\sigma = 0$ to give $\sigma^e_{(t)} = \sigma_o exp(-E\eta^{-1}t)$ from which dashpot displacement can be derived using the relationship $\dot{\varepsilon}^D = \dot{\delta}^D/l_o = \sigma/\eta$, which integrates to give $\delta^D_{(t)} = \delta^e_{(0)}\left(1 - exp(-E\eta^{-1}t)\right)$. It is now a relatively simple matter to determine the energy stored elastically (area A_1 in figure A-1) which is $W^e_{(t)} = 0.5\sigma_{(t)}\delta^e_{(t)}$ and the energy dissipated by the dashpot which is obtained from the change in the work done at the dashpot $\dot{U}_D = \dot{W}^D_d$, integration of $\dot{U}_D = l_o\sigma^D_{(t)}\dot{\varepsilon}^D$ and divided by the area the dissipated energy at the dashpot per unit area is evaluated.

$$W^D_{(t)} = \frac{U_D}{A} = \int_0^t \eta l_o (\dot{\varepsilon}^D)^2\, dt = \frac{1}{2}\sigma^e_{(0)}\delta^e_{(0)}\left(1 - \left(exp\left(\frac{-E}{\eta}t\right)\right)^2\right) \tag{A1}$$

$$W^d_{(t)} = W^e_{(t)} + W^D_{(t)} \tag{A2}$$

Things are slightly more involved if $\sigma_o > \sigma_c$ as the cohesive element must be accounted for and it is assumed to respond instantaneously with $\delta_o = \delta^e_{(0)} + \delta$, where $\delta^e_{(0)}$ is the bulk material response and δ arises from the cohesive element. Since stress is common to both the elastic bulk material and the cohesive element the equality $\sigma^e_{(0)} = \sigma_c(1 - \delta/\delta_c) = E\,\delta^e_{(0)}/l_o$ applies, which solves to give

$$\sigma^e_{(0)} = \frac{E\delta_c}{l_o}\left[\frac{\left(1-\frac{\delta_o}{\delta_c}\right)}{\left(-1+\frac{E\delta_c}{\sigma_c l_o}\right)}\right] \tag{A3}$$

which is applicable for $\delta_o \leq \delta_c$ as otherwise the element will fail and the material will separate. With $\sigma^e_{(0)}$ known the subsequent behaviour follows with $\sigma^e_{(t)} = \sigma^e_{(0)}\, exp(-E\eta^{-1}t)$ and $\delta^e_{(t)} = \delta^e_{(0)}\, exp(-E\eta^{-1}t)$ along with energies associated with each element, i.e.

$$W^e_{(t)} = A_1 = \frac{1}{2}\sigma^e_{(t)}\delta^e_{(t)} \tag{A4}$$

$$W_\Gamma = A_2 = \frac{1}{2}\left(\sigma_c + \sigma^e_{(0)}\right)\left(\delta_a - \delta^e_{(0)}\right) + \frac{1}{2}\left(\sigma_c + \sigma^e_{(0)}\right)(\delta_0 - \delta_a)$$

$$= \frac{1}{2}\left(\sigma_c + \sigma^e_{(0)}\right)\delta \tag{A5}$$

which provides

$$W_{(t)}^{\mathrm{d}} = W_{(t)}^{\mathrm{e}} + W_{(t)}^{\mathrm{D}} + W_{\Gamma} \tag{A6}$$

with $W_{(t)}^{D}$ obtained from Eq (A1).

List of symbols

Γ_o	Critical cohesive energy
Γ_{rate}	Rate-dependent cohesive energy
σ_c	Critical cohesive stress
δ_c	Critical separation
δ_o	Instantaneous applied displacement
δ_1	Shape parameter for the linear and trapezoidal model respectively
δ_2	Second shape parameter of the trapezoidal model
δ^{p}	Plastic separation
δ^{e}	Elastic separation
δ_f	Final separation at fracture
δ^{coh}	Separation in the cohesive element
$\dot{\delta}$	Separation rate
$\dot{\delta}^D$	Separation rate at the dashpot
σ	Cohesive stress
σ_Y	Yield stress
ϑ	Poisson's ratio
σ^D	Stress at the dashpot
E	Elastic modulus
E^{p}	Plastic modulus
C_{R}	Rayleigh surface wave speed
G_{c}	Total dissipated energy per unit area
G^{p}	Dissipated plastic energy in the cohesive zone per unit area

$G^{p_{rate}}$	Rate-dependent plastic dissipated energy in the cohesive zone per unit area
$\varepsilon^{\mathrm{coh}}$	Strain at the cohesive zone
ε^{e}	Elastic strain
W^{e}	Elastic strain energy per unit area
W^{Γ}	Dissipated energy per unit area due to the fracture process
W^{p}	Dissipated energy per unit area due to plastic deformation in the bulk material
W^{d}	Total work done per unit area by the external load
W^{D}	Dissipated energy per unit area in the dashpot
η	Material viscosity
B	Parameter representing the rate dependency of the cohesive material
B_1	Parameter representing the rate dependency of the cohesive material
σ_c^{rate}	Rate-dependent critical stress
δ_c^{rate}	Rate-dependent critical separation
δ_{max}	The separation at the onset of unloading
σ_{max}	The stress at the onset of unloading
σ_{limit}	Upper limit on the rate-dependent critical stress
$W_{limit}^{\Gamma_{\mathrm{rate}}}$	Upper limit on the rate-dependent fracture energy

Abbreviation

CZ	Cohesive zone
CE	Cohesive element
CZM	Cohesive zone model
BCZM	Bilinear cohesive zone model
TCZM	Trapezoidal cohesive zone model
LEFM	Linear cohesive zone model

TSL	Traction separation law
QS-B	Quasi-static simulation using the rate-independent bilinear model
QS-T	Quasi-static simulation using the rate-independent trapezoidal model
DYN-σ_c^{rate}-B	Dynamic simulation using the stress rate-dependent bilinear model
DYN-σ_c^{rate}-T	Dynamic simulation using the stress rate-dependent trapezoidal model
DYN-δ_c^{rate}-B	Dynamic simulation using the separation rate-dependent bilinear model
DYN-Γ_c^{rate}-B	Dynamic simulation using the new rate-dependent bilinear model
DYN-Γ_c^{rate}-T	Dynamic simulation using the new rate-dependent trapezoidal model

Table(s)

Table 1. material properties and process parameters

Length $\boldsymbol{l_o}$ mm	$\boldsymbol{\sigma_c}$ MPa	$\boldsymbol{\delta_c}$ mm	$\boldsymbol{\sigma_Y}$ MPa	$\boldsymbol{\Gamma_0}$ N/mm	E MPa	$\boldsymbol{E^p}$ MPa	$\boldsymbol{\delta_1}$ mm
10	340	0.17647	300	30	72000	1390	0

$\boldsymbol{\delta_2}$ mm	Viscosity (η) Pa.s			B s/m	B_1 s/m	separation rate ($\dot{\delta}$) m/s		
$0.5\boldsymbol{\delta_c}$	10	30	60	0.1	0.02	5	10	20

Table(s)

Table 2. Type of simulations applied to a standard CT specimen

Model	Analysis type	Bulk material response	Cohesive Zone response	TSL	Number of simulations
QS-B	Quasi-static	Rate-independent	Standard	BCZM	2
QS-T	Quasi-static	Rate-independent	Standard	TCZM	7
DYN -B	Transient dynamic	Rate-independent	Standard	BCZM	4
DYN -T	Transient dynamic	Rate-independent	Standard	TCZM	4
DYN-$\boldsymbol{\sigma}_c^{\mathbf{rate}}$-B	Transient dynamic	Rate-independent	Rate-dependent	BCZM	7
DYN-$\boldsymbol{\sigma}_c^{\mathbf{rate}}$-T	Transient dynamic	Rate-independent	Rate-dependent	TCZM	5
DYN-$\boldsymbol{\delta}_c^{\boldsymbol{rate}}$-B	Transient dynamic	Rate-independent	Rate-dependent	BCZM	4
DYN-$\boldsymbol{\Gamma}_c^{\mathbf{rate}}$-B	Transient dynamic	Rate-independent	Rate-dependent	BCZM	5
DYN-$\boldsymbol{\Gamma}_c^{\mathbf{rate}}$-T	Transient dynamic	Rate-independent	Rate-dependent	TCZM	5

Table(s)

Table 3. Cohesive model parameters

Cohesive parameter set	Cohesive law	Γo (N/m)	E^{coh} (GPa)	$\boldsymbol{\sigma_c}$ (Pa)	$\boldsymbol{\delta_c}$ (m)	$\boldsymbol{\delta_1}$ (m)	$\boldsymbol{\delta_2}$ (m)
1	BCZM	189000	15000	6.0e8	0.00063	0.00004	0.00004
	TCZM	189000	15000	6.0e8	0.00038286	0.00004	0.000287145
2	BCZM	189000	15000	6.0e8	0.00063	0.00004	0.00004
	TCZM	189000	15000	3.5e8	0.00063	0.000023	0.0004725
3	BCZM	189000	15000	6.0e8	0.00063	0.00004	0.00004
	TCZM	246500	15000	4.6e8	0.00063	0.0000307	0.0004725
4	TCZM	222000	15000	3.1e8	0.00083	0.0000207	0.0006225

Figure(s)

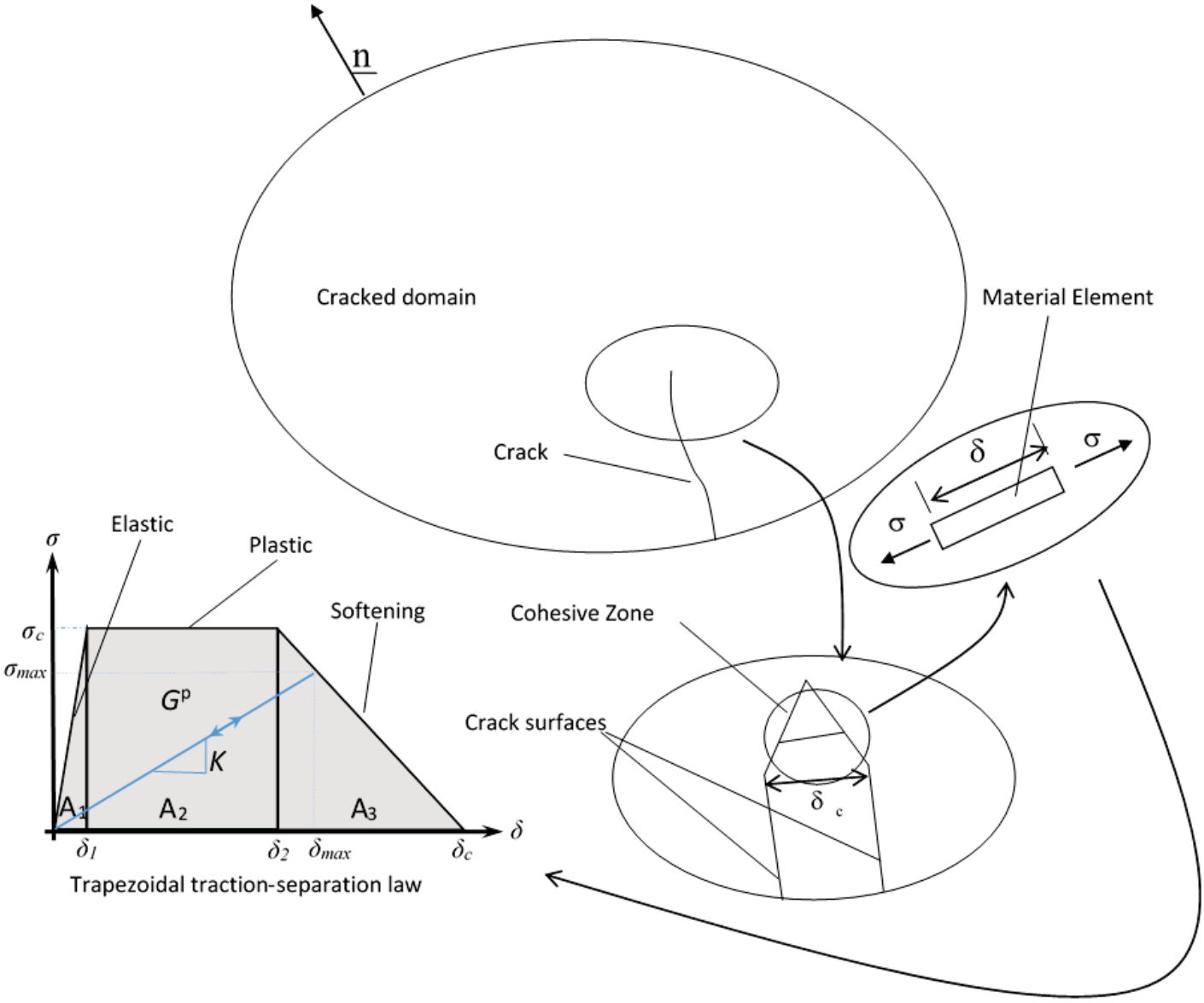

Figure 1. Mode I Cohesive Zone model

Figure(s)

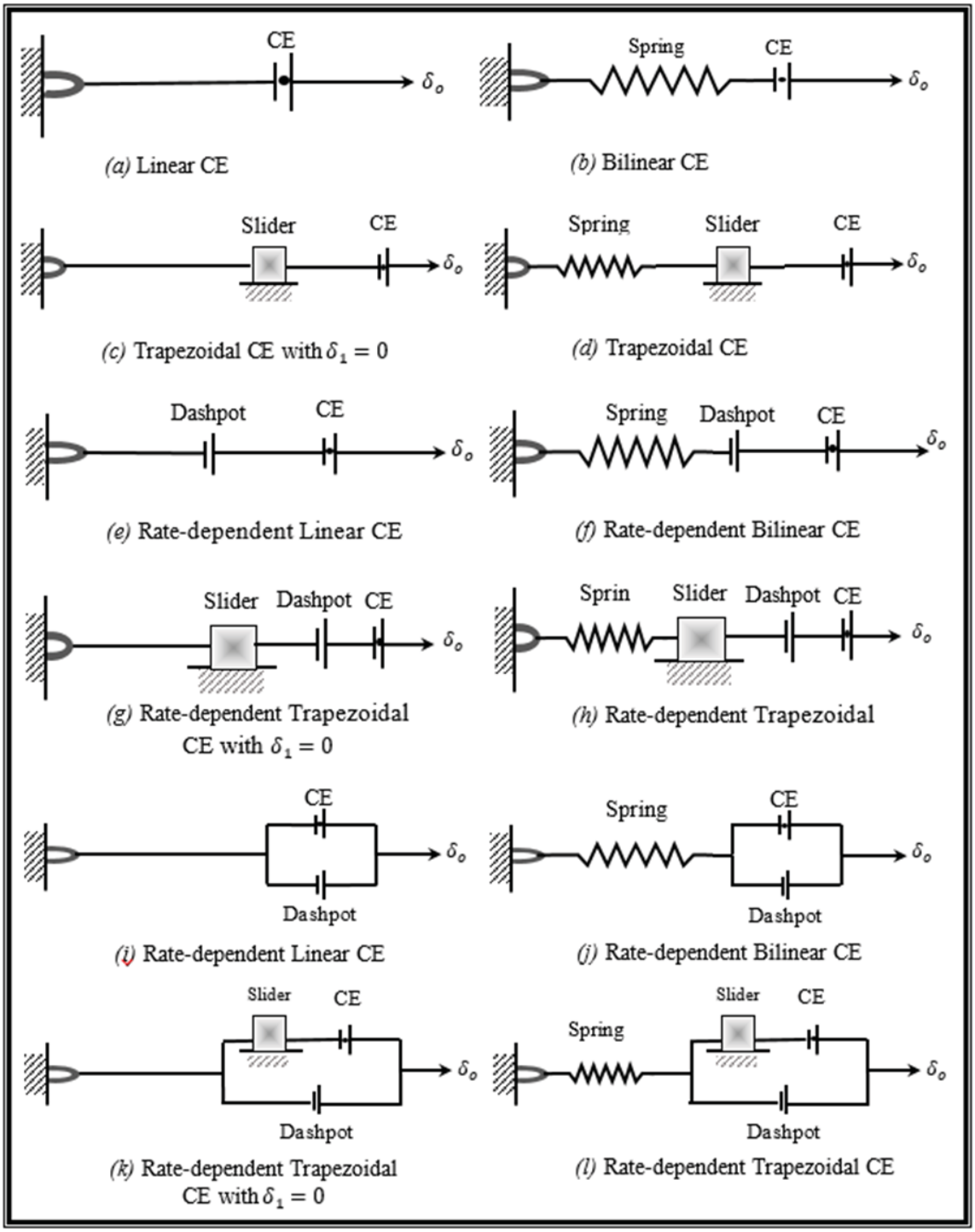

Figure 2. Elementary Material Elements in the Cohesive-Zone

Figure(s)

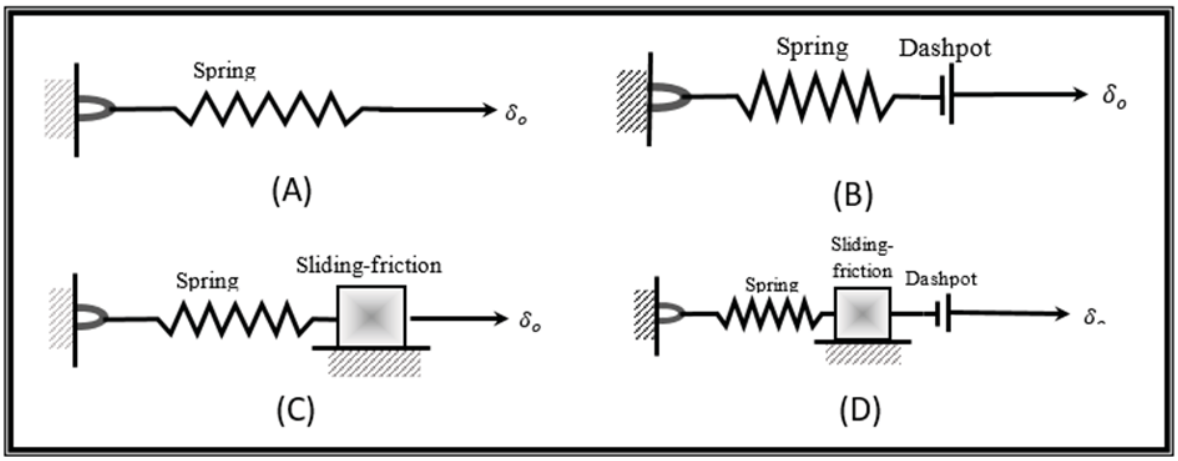

Figure 3. Elementary Bulk-Material Models

Figure(s)

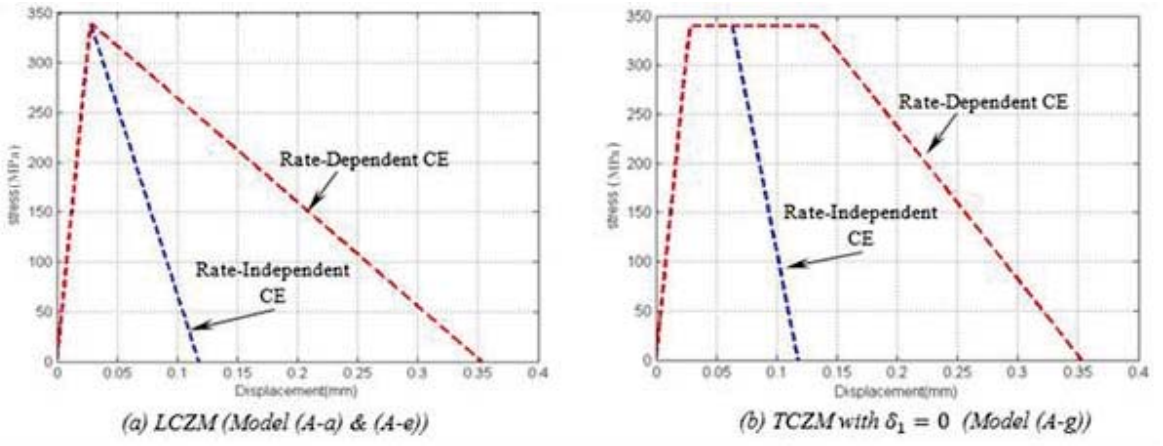

Figure 4. Stress-displacement curve for the cohesive element in an elastic bulk material

Figure(s)

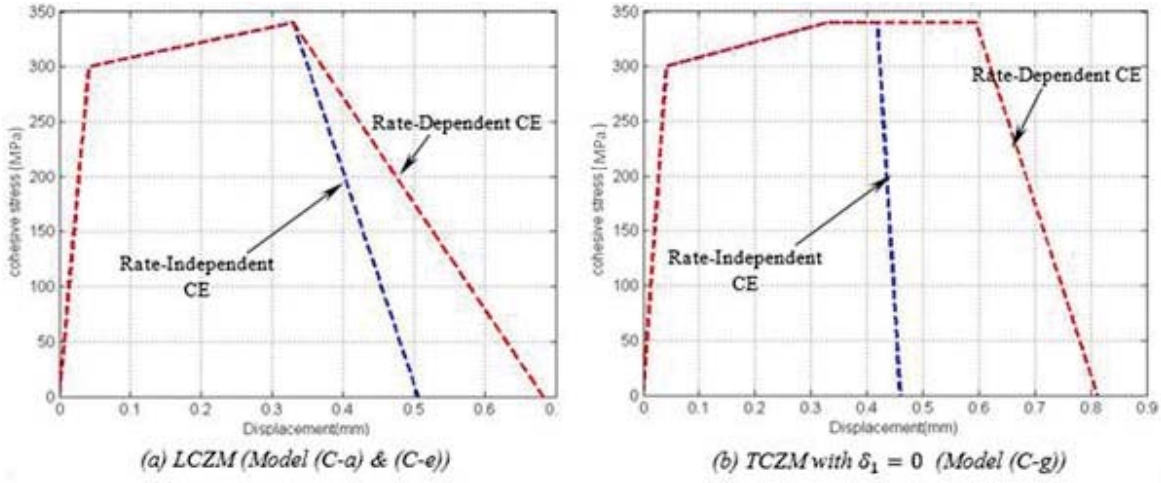

Figure 5. Stress-displacement curve for the cohesive element in an elastic-plastic bulk material

Figure(s)

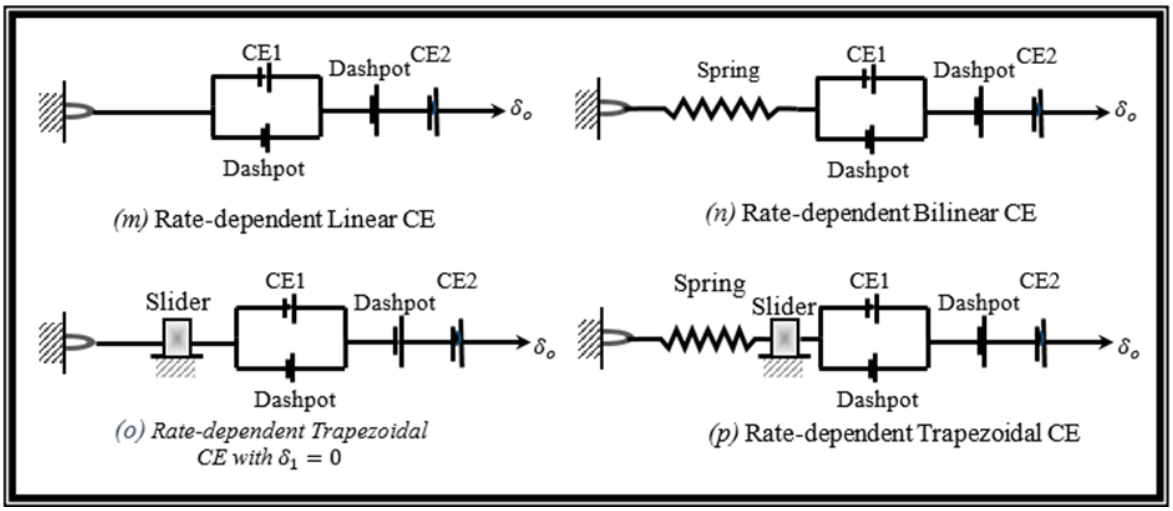

Figure 6. New Elementary Rate-dependent Material Element in the Cohesive Zone

Figure(s)

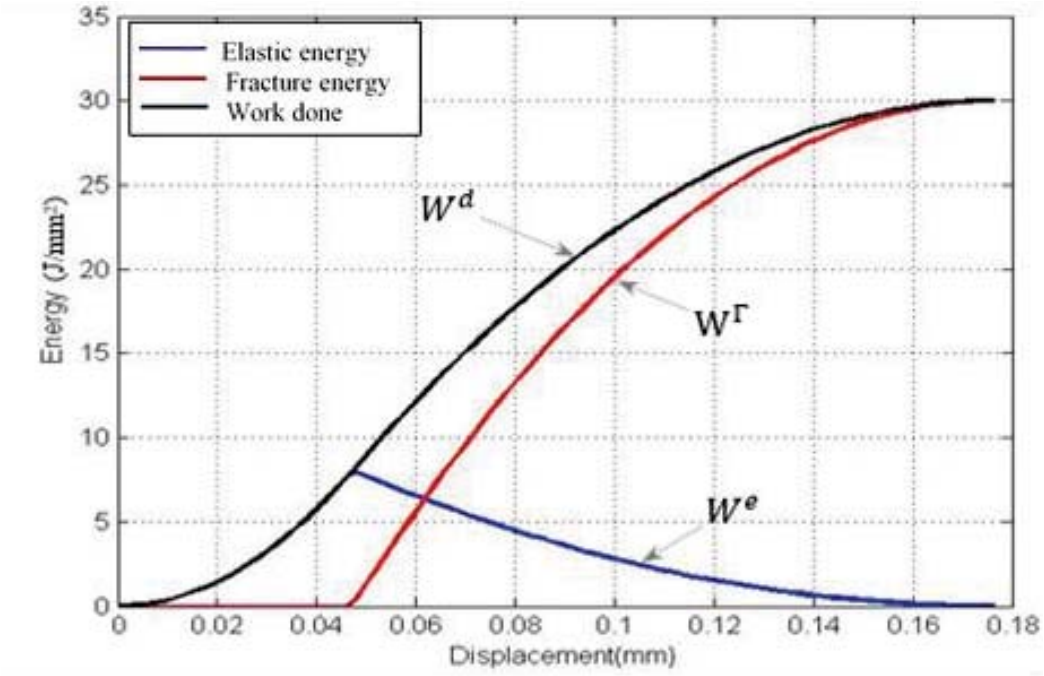

Figure 7. Model (A-a) energy-displacement curve of a rate-independent CE in an elastic bulk material

Figure(s)

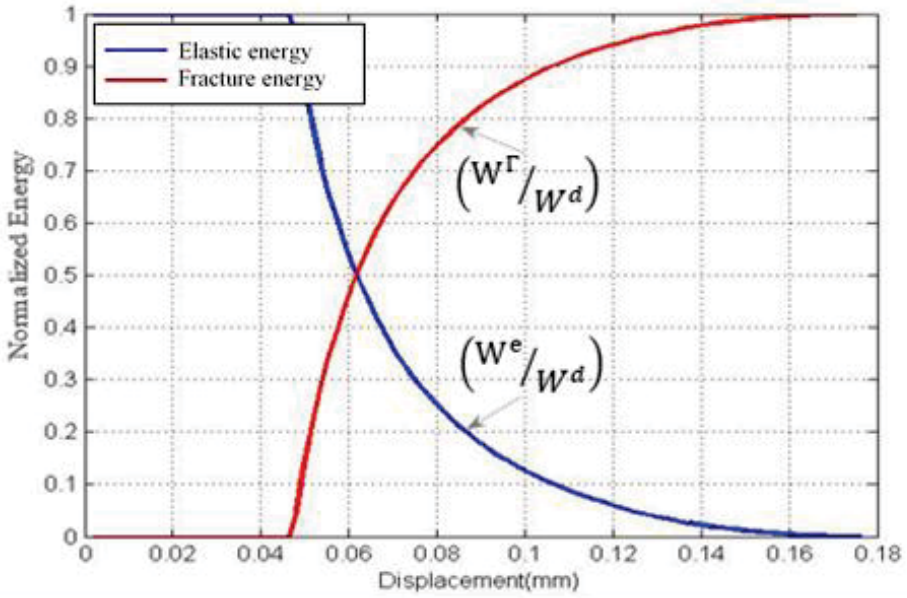

Figure 8. Model (A-a) normalized elastic and fracture energy diagram

Figure(s)

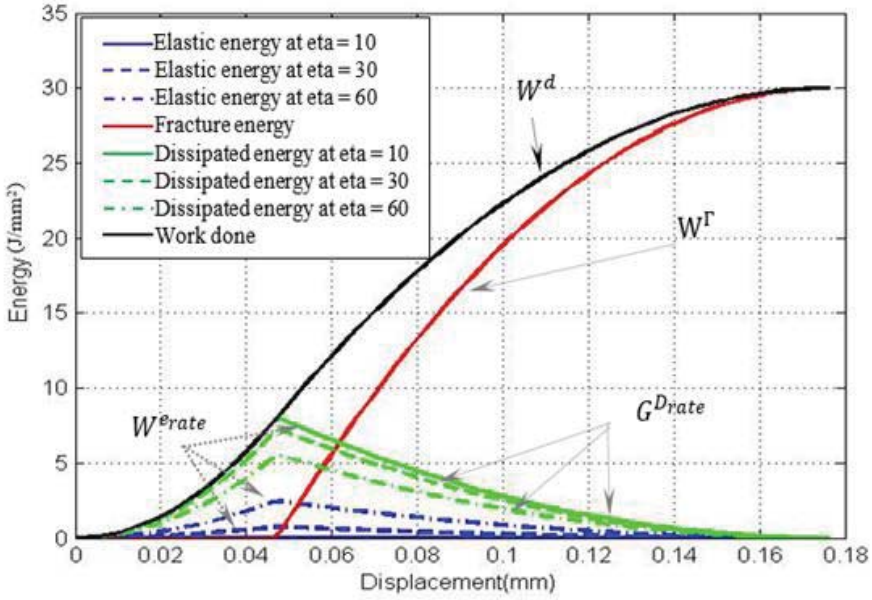

Figure 9. Model (B-a) material relaxation response.

Figure(s)

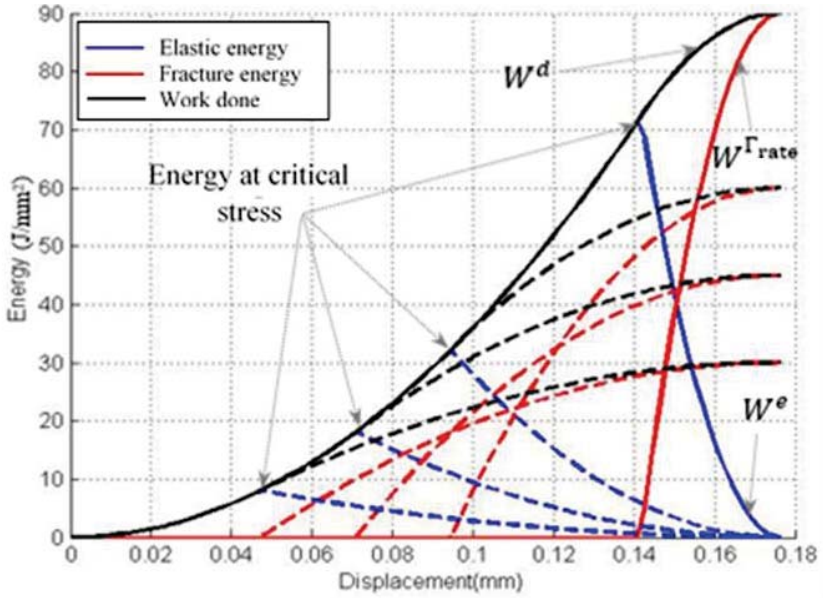

Figure 10.The increase in the value of energy at critical stress due to unrealistic increasing critical cohesive stress in Model (A-i)

Figure(s)

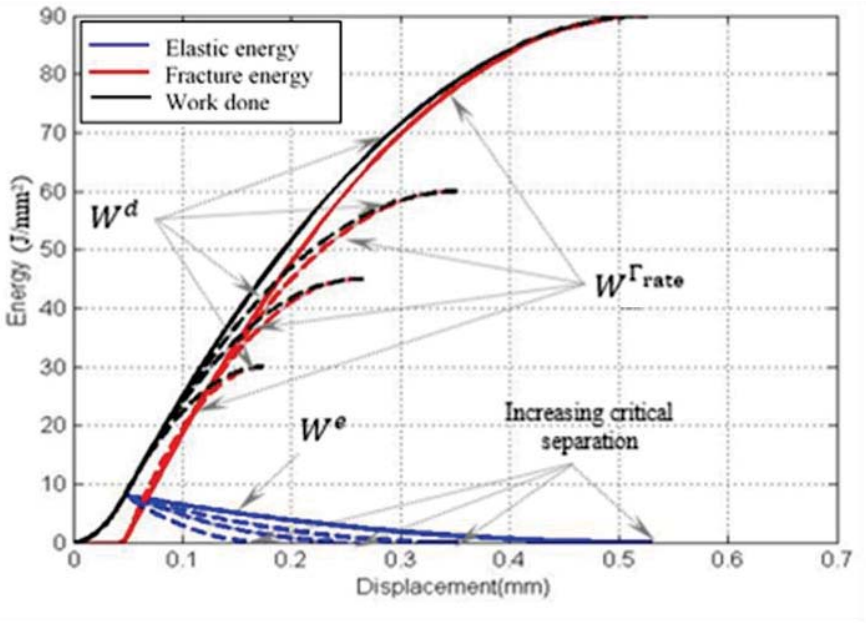

Figure 11. The unrealistic increasing critical cohesive separation in Model (A-e)

Figure(s)

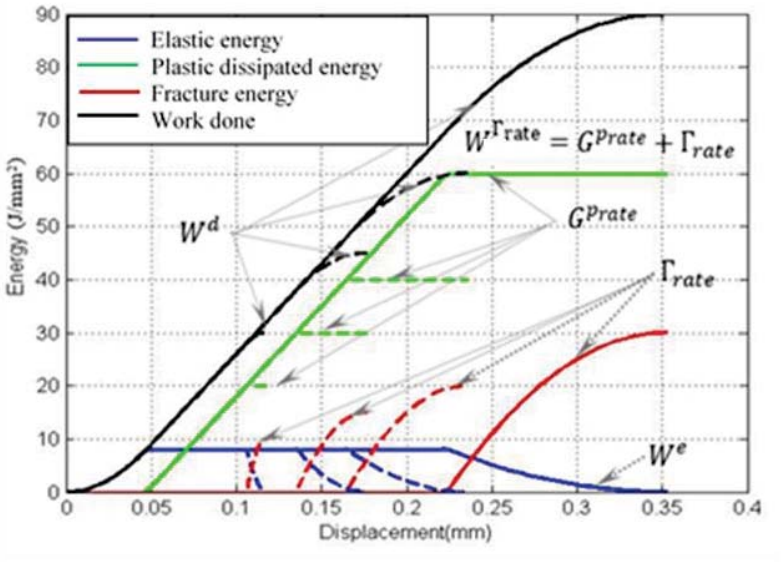

Figure 12. Model (A-g) plasticity capture locally by using the trapezoidal rate-dependent CE

Figure(s)

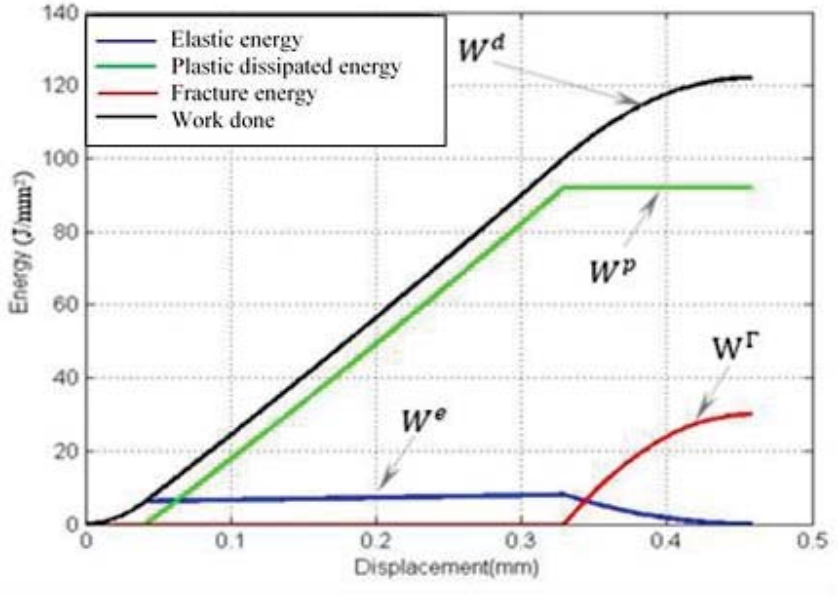

Figure 13. Model (C-a) energy-displacement curve of a rate-independent CE in an elastic-plastic bulk material

Figure(s)

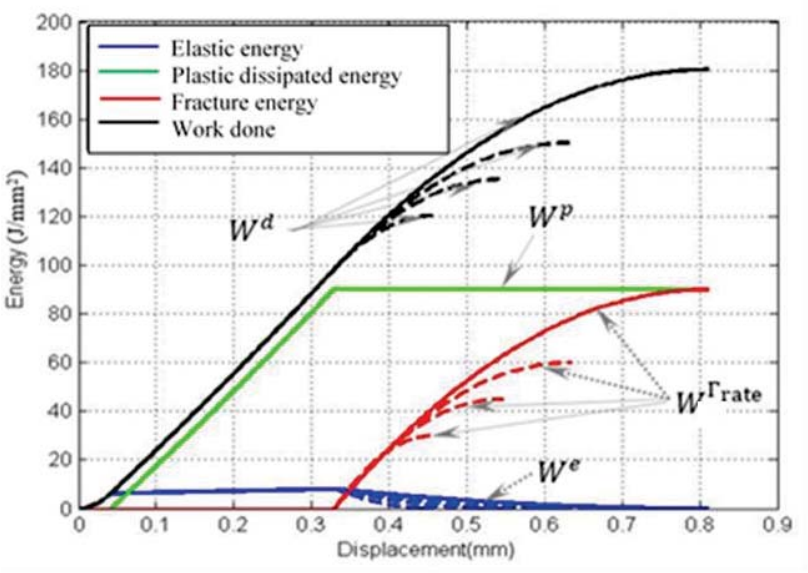

Figure 14. Model (C-e) linear rate-dependent CE in an elastic-plastic material

Figure(s)

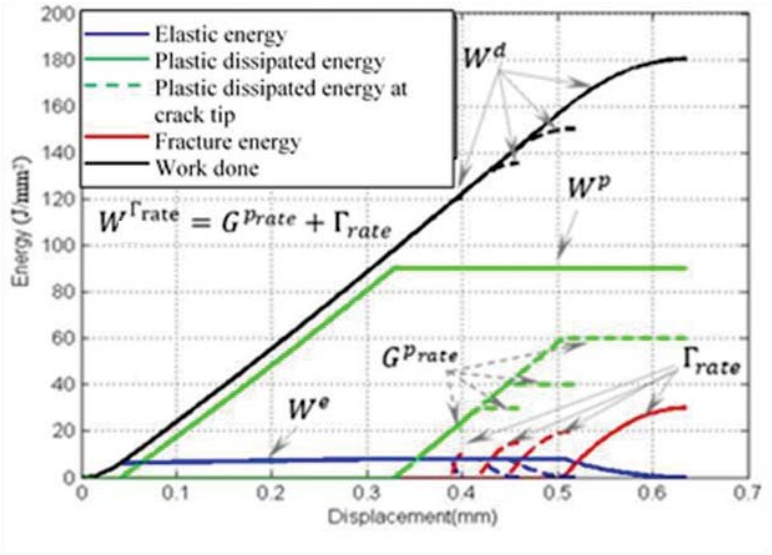

Figure 15. Model (C-g) trapezoidal rate-dependent CE in an elastic-plastic material

Figure(s)

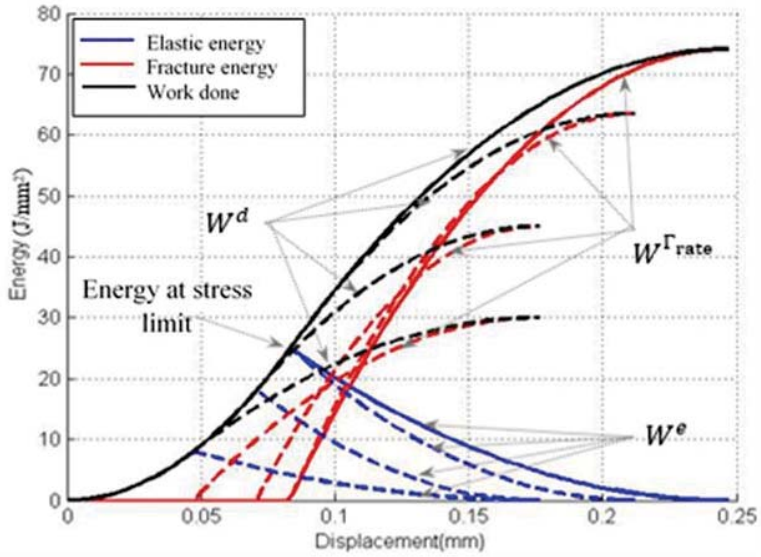

Figure 16. Model (C-m) effect of stress limit in the new linear rate-dependent CE in an elastic bulk material

Figure(s)

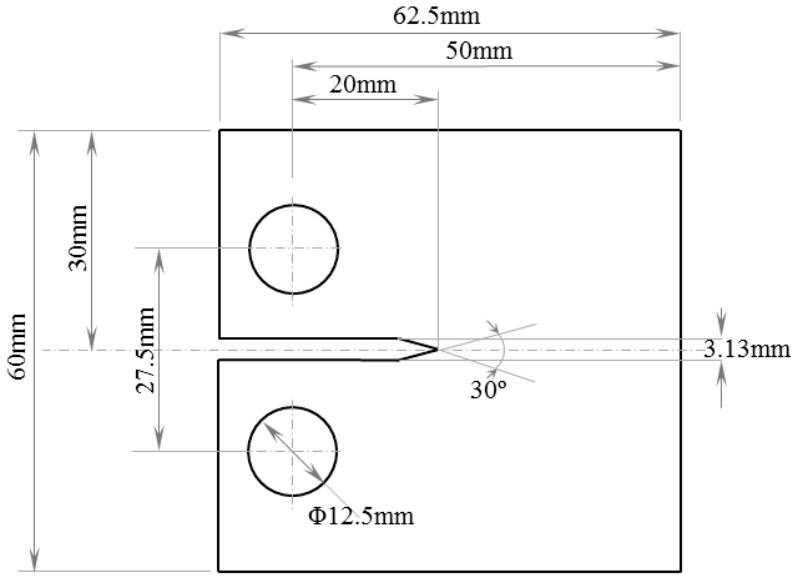

Figure 17. CT specimen dimensions

Figure(s)

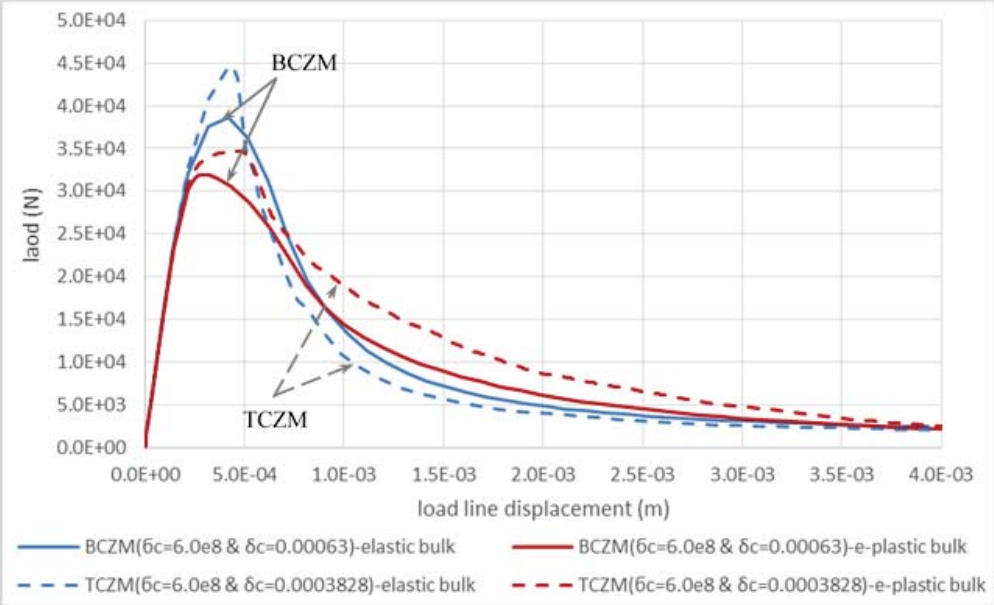

Figure 18. Load versus load line displacement for the BCZM & TCZM with equal fracture energy (189 N/mm) and critical stress

Figure(s)

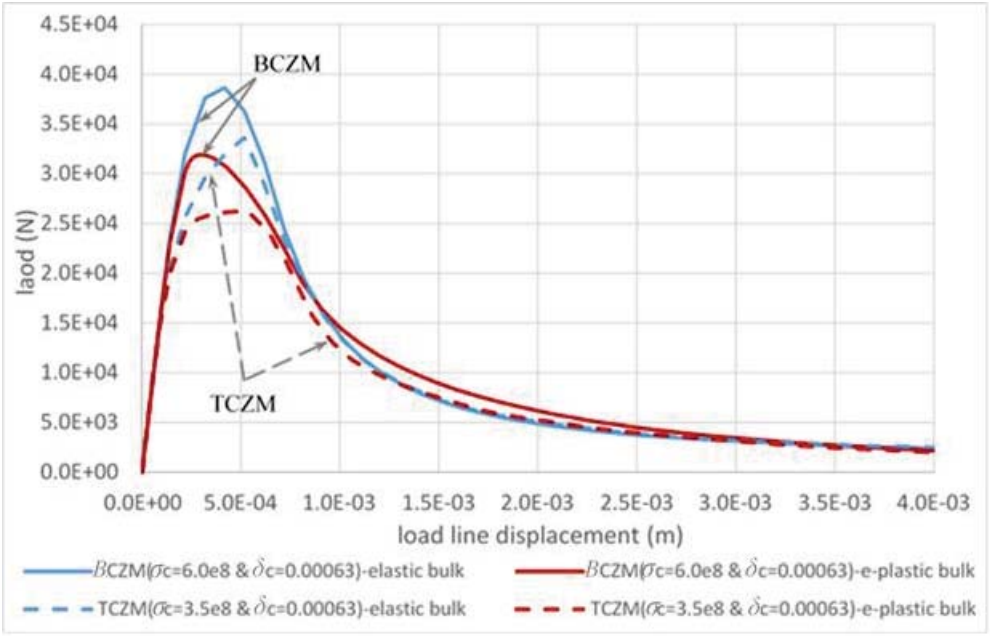

Figure 19. Load versus load line displacement for the BCZM & TCZM with equal critical fracture energy (189 N/mm) and critical separation

Figure(s)

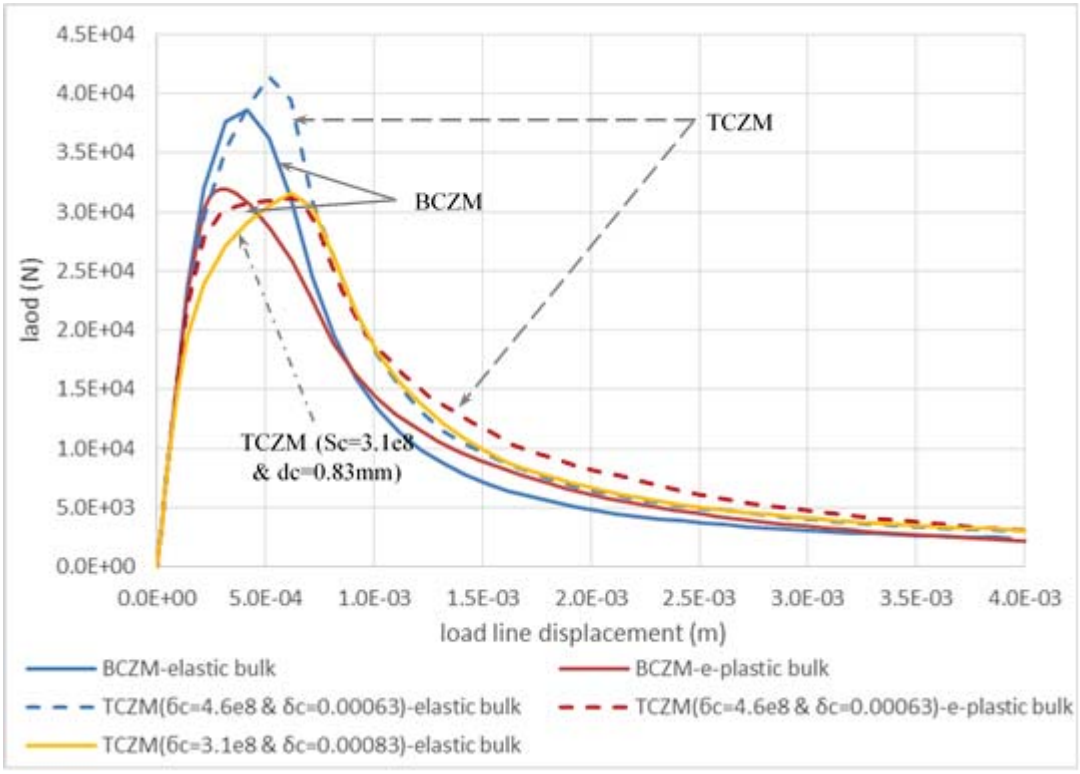

Figure 20. Load versus load-line displacement for the BCZM & TCZM

Figure(s)

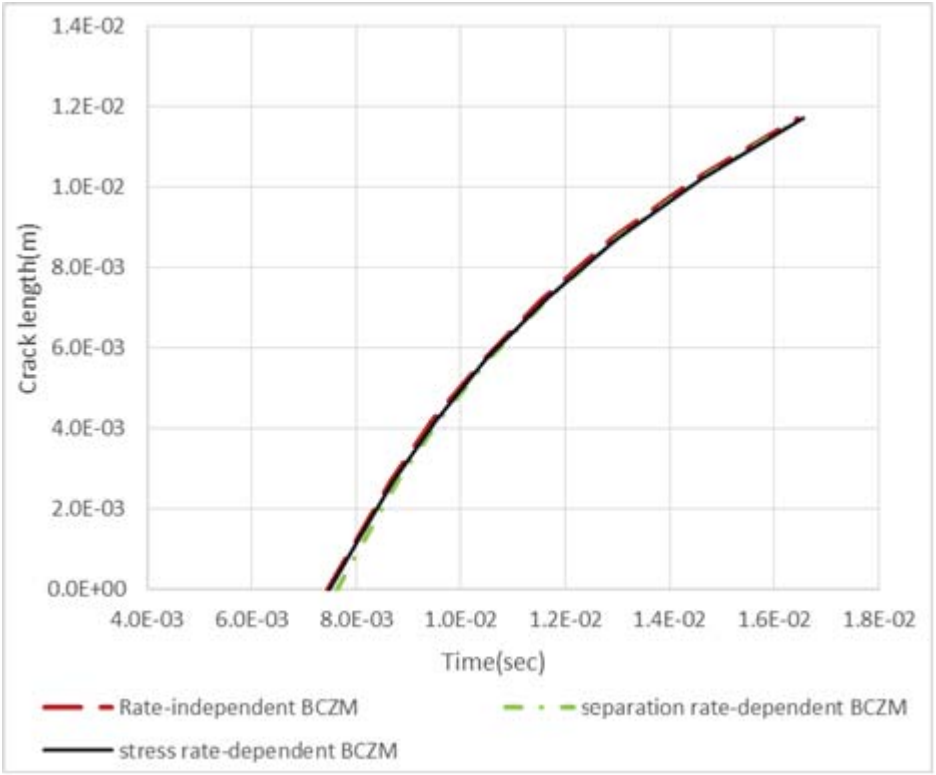

Figure 21. Crack length-time curve for the 0.1 m/s loading speed under displacement control

Figure(s)

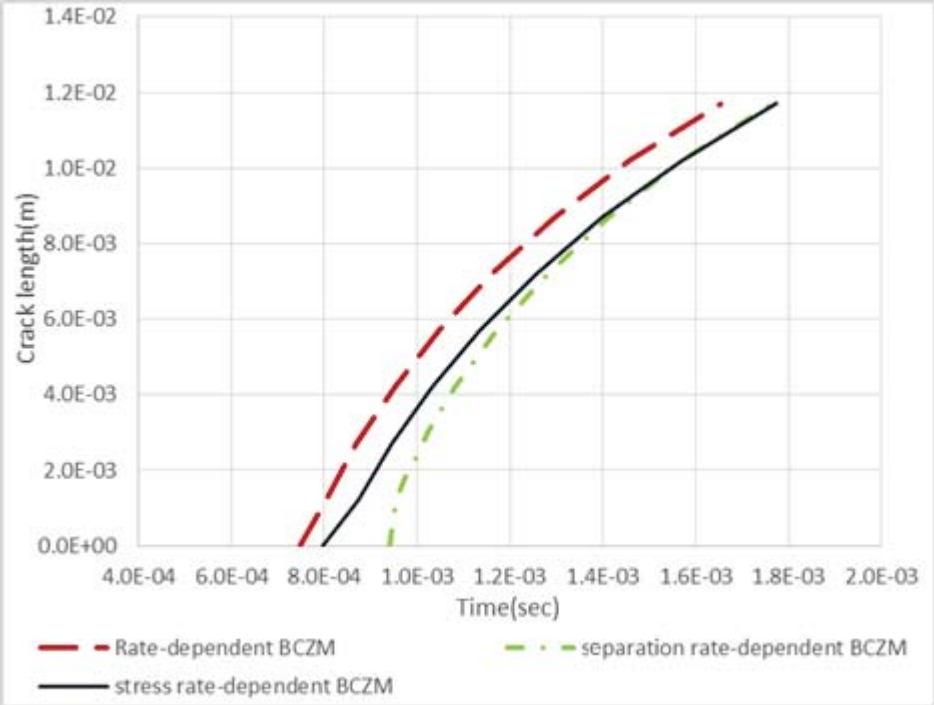

Figure 22. Crack length-time curve for the 1 m/s loading speed under displacement control

Figure(s)

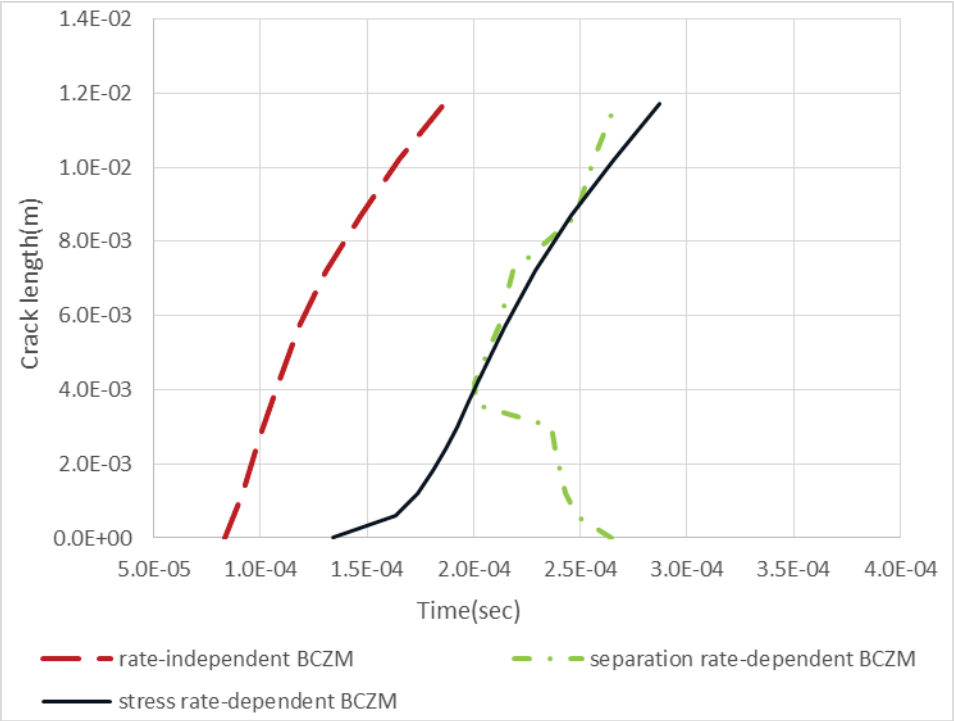

Figure 23. Crack length-time curve for the 10 m/s loading speed under displacement control

Figure(s)

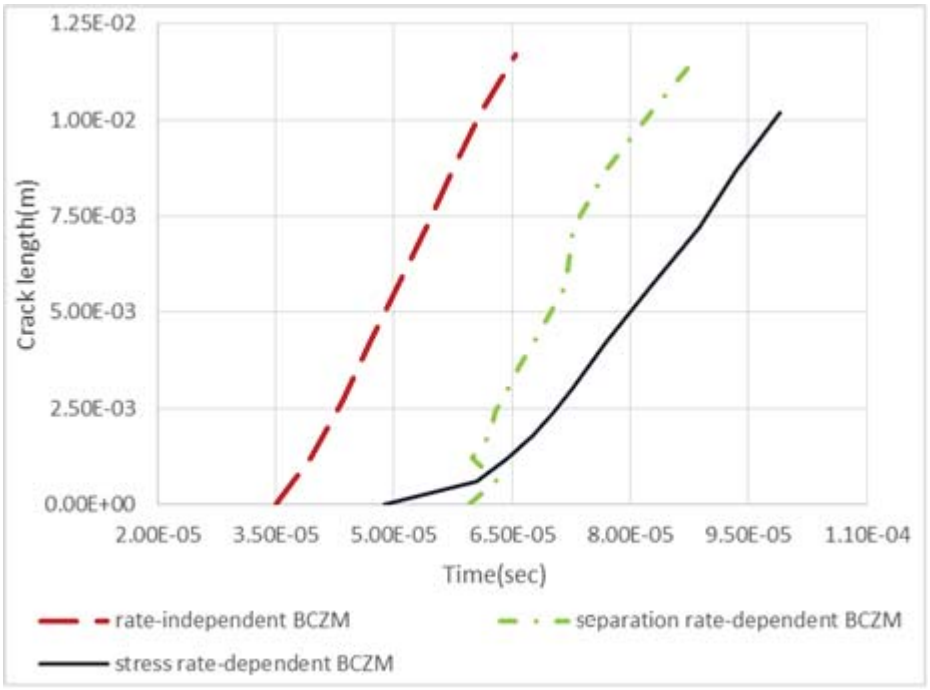

Figure 24. Crack length-time curve for the 100 m/s loading speed under displacement control

Figure(s)

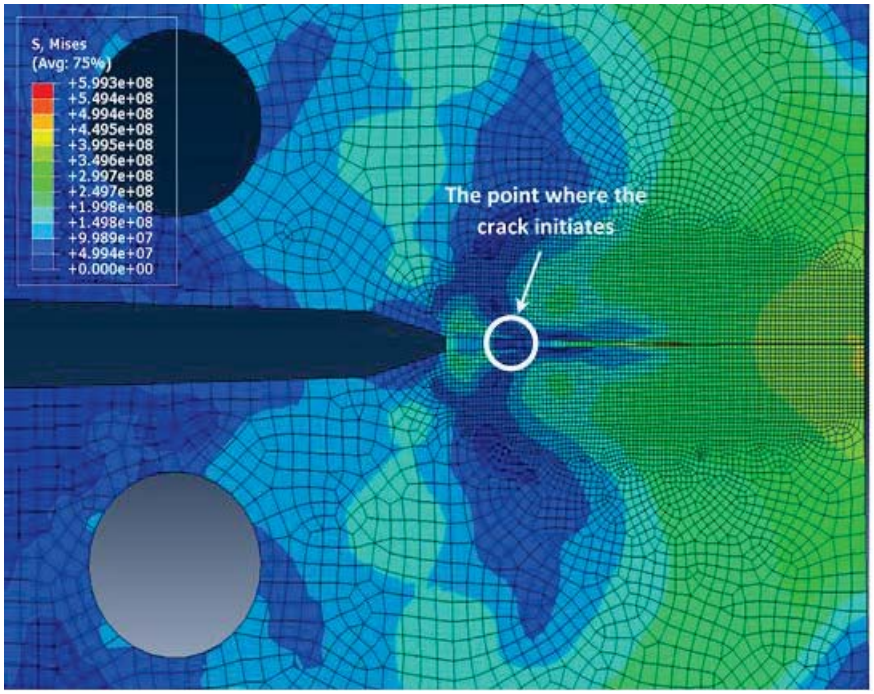

Figure 25. The crack initiation point of the separation rate-dependent model at 10 m/s loading speed

Figure(s)

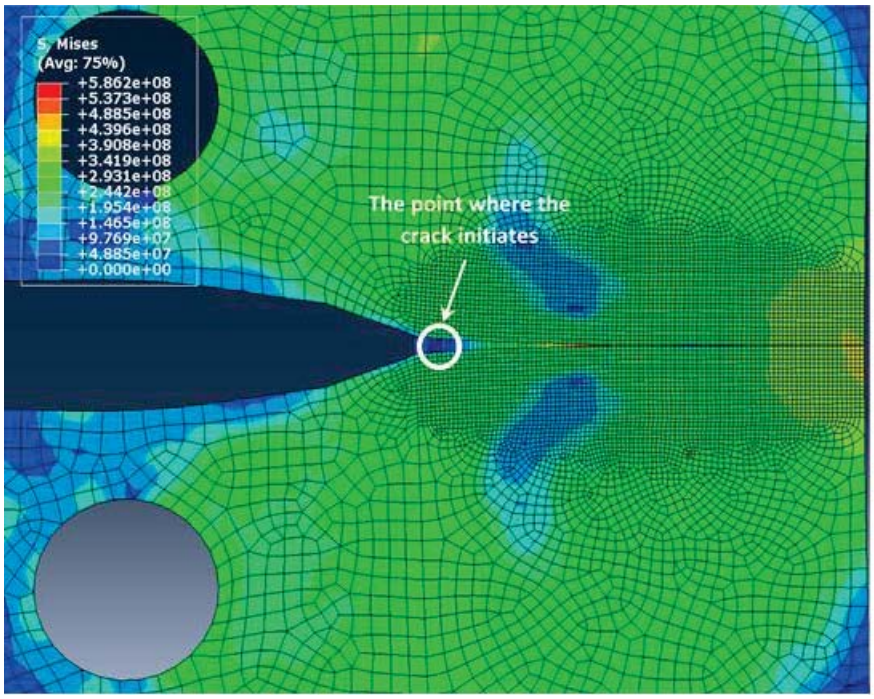

Figure 26. The crack initiation point of the separation rate-dependent model at 100 m/s loading speed

Figure(s)

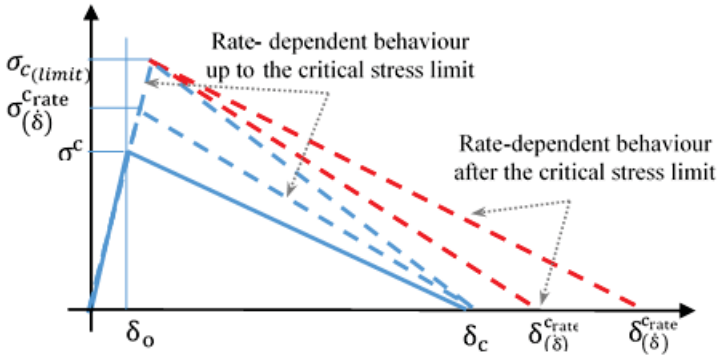

Figure 27. Stress-displacement curve of the new rate-dependent model

Figure(s)

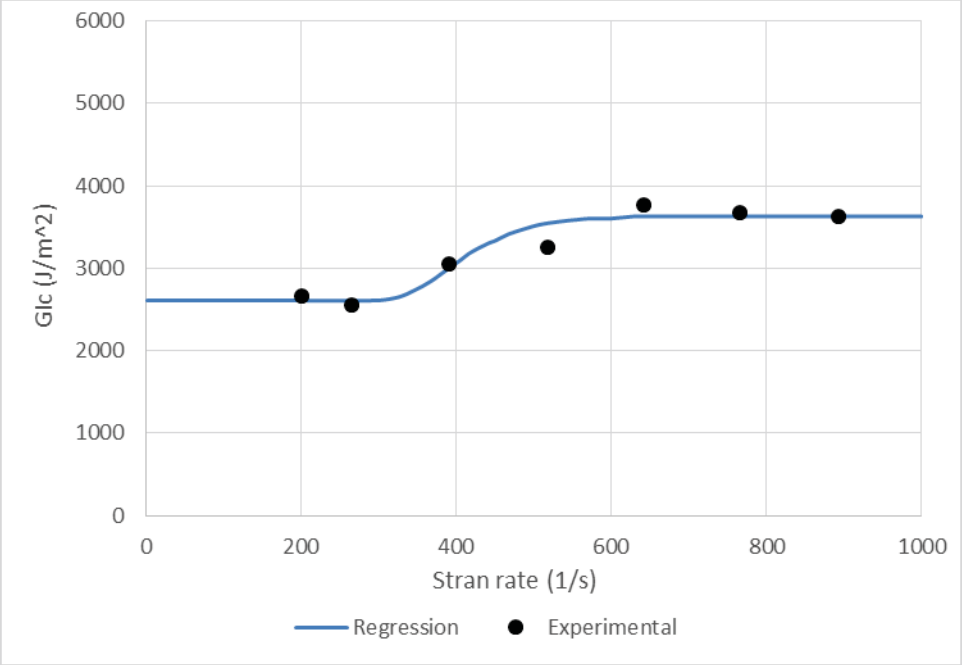

Figure 28. Experimental energy-strain rate curve[28]

Figure(s)

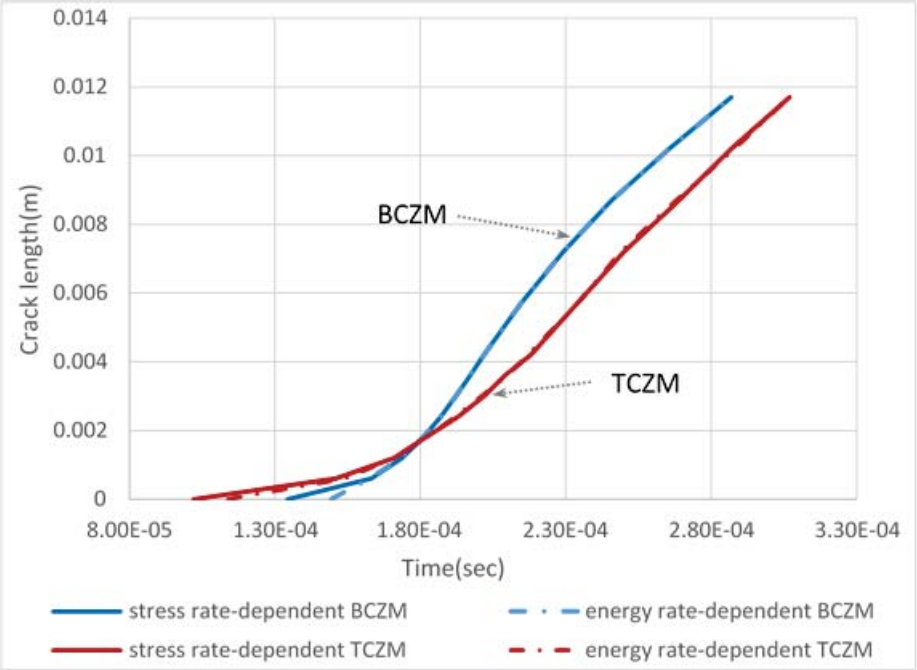

Figure 29. Crack length as a function of the time at (B=0.7 & B1=0.126) at 10m/s loading speed

Figure(s)

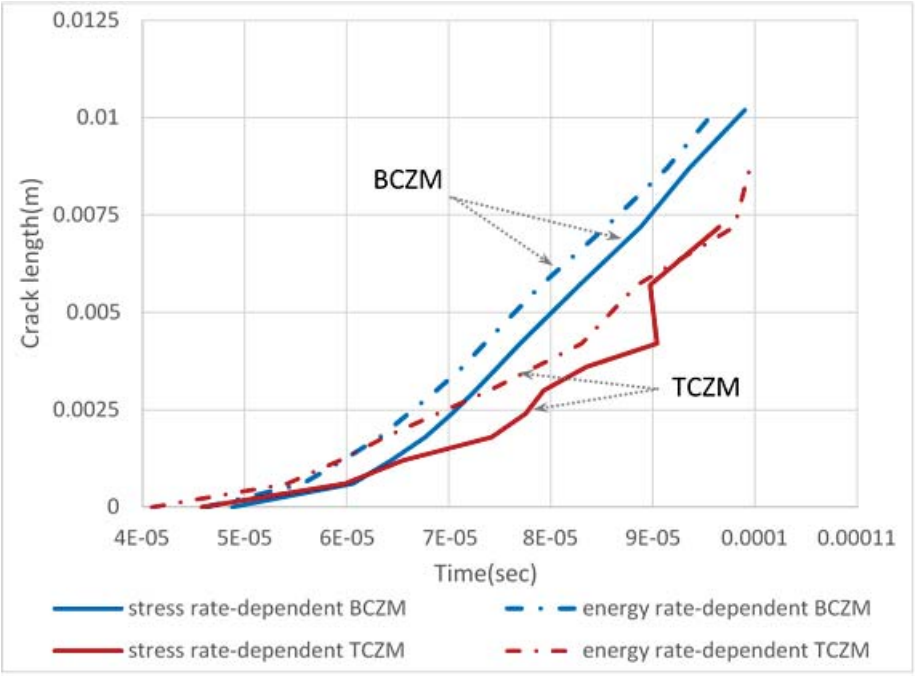

Figure 30. crack length as a function of the time at (B=0.7 & B1=0.126) at 100m/s loading speed

Figure(s)

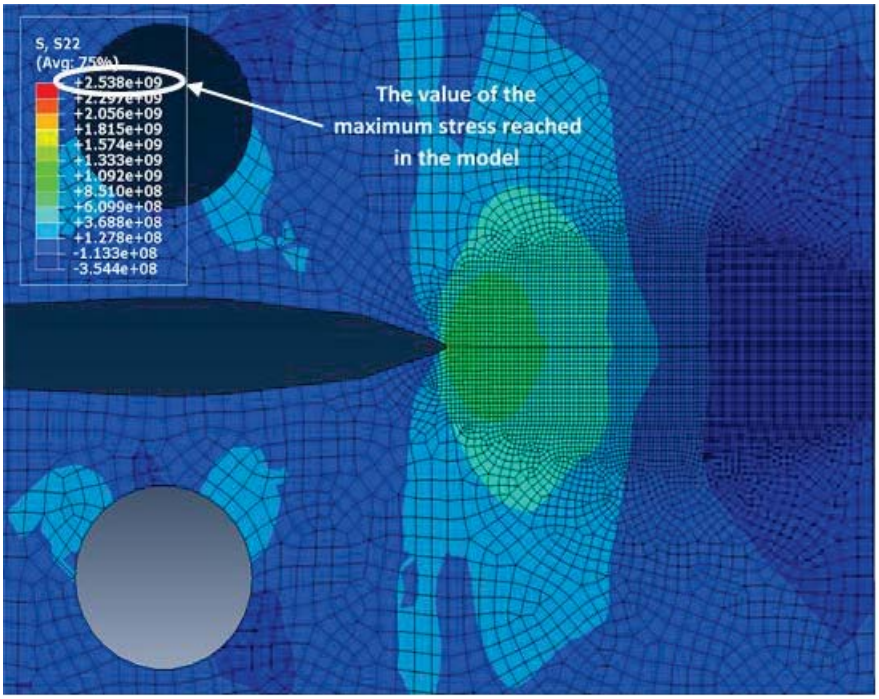

Figure 31. The maximum stress reached by using the stress rate-dependent model under displacement control at 10 m/s loading speed

Figure(s)

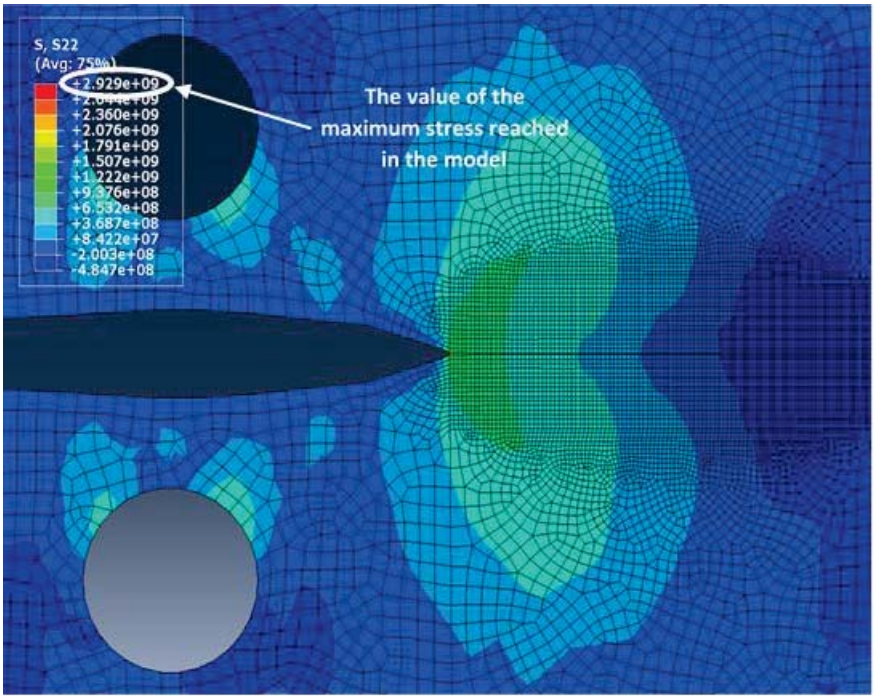

Figure 32. The maximum stress reached by using the stress rate-dependent model under displacement control at 100 m/s loading speed

Figure(s)

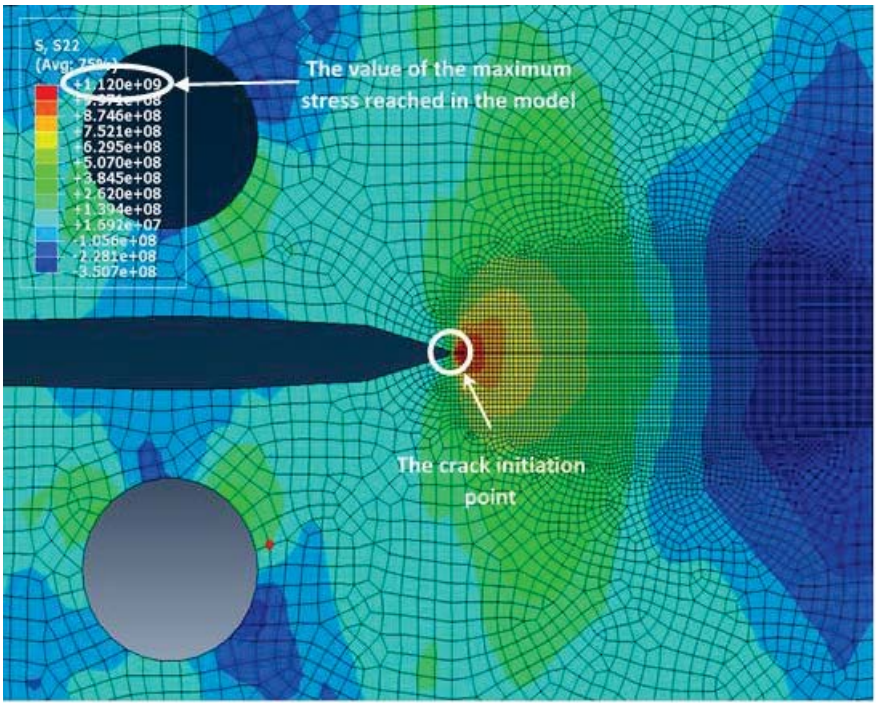

Figure 33. The maximum stress and the point of crack initiation by using the new rate-dependent model under displacement control at 100 m/s loading speed

Figure(s)

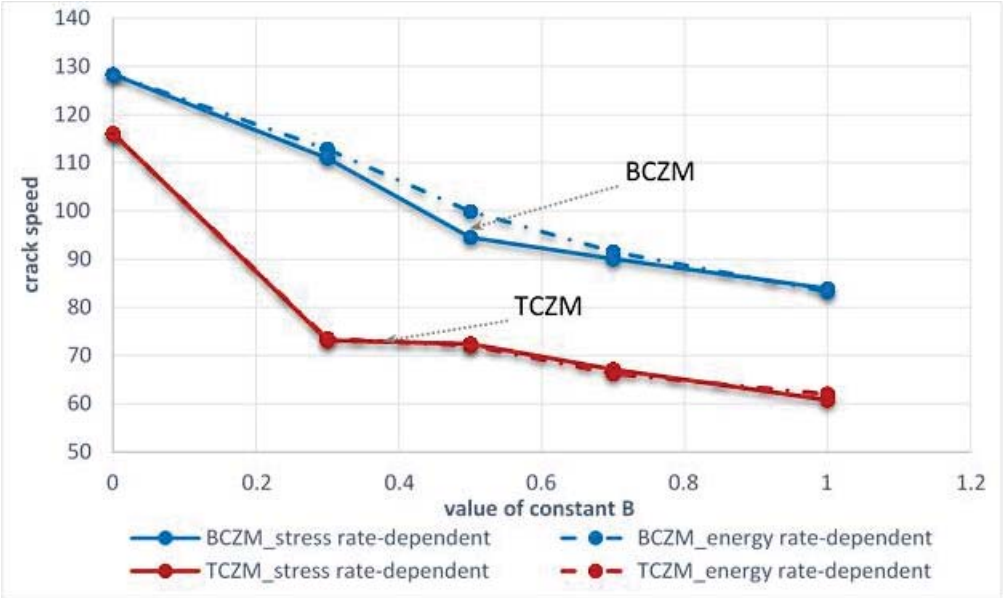

Figure 34. Crack speed as a function of the parameter B at 10m/s loading speed

Figure(s)

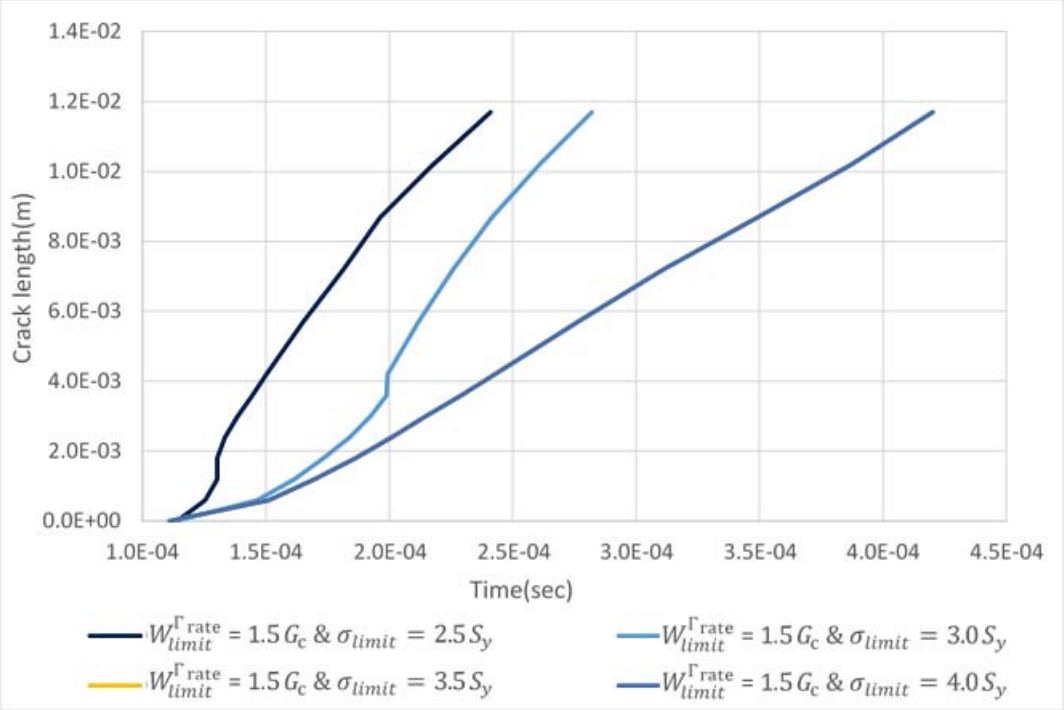

Figure 35. The effect of applying a high value for σ_{limit} compared with the value evaluated from $W_{limit}^{\Gamma rate}$

Figure(s)

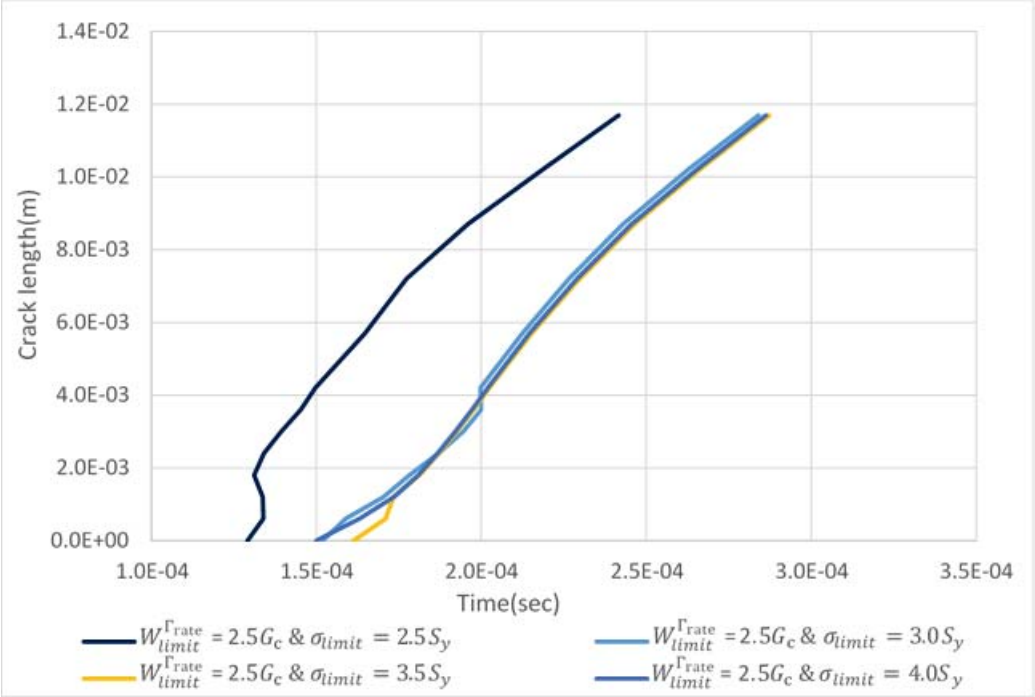

Figure 36. The effect of applying a value for σ_{limit} close to the value evaluated from $W_{limit}^{\Gamma_{rate}}$

Figure(s)

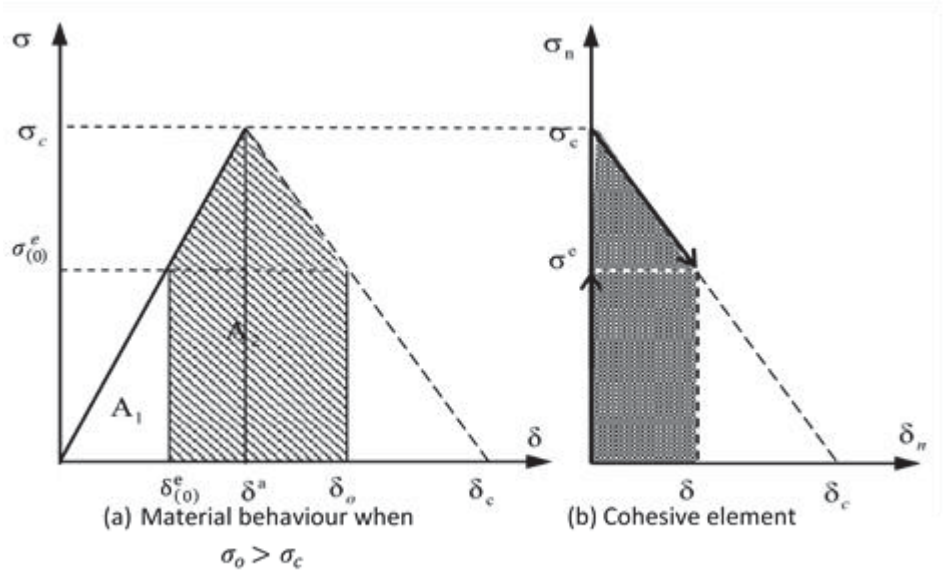

Figure A-1 Elastic and fracture energy for an elastic material